AN ABSTRACT OF THE THESIS OF

Rainer Ludwig for the degree of Master of Science in Geophysics presented on November 3, 1989

Title: Double Subduction beneath Hispaniola? An Investigation of Earthquakes by Body Wave Inversion.

Redacted for Privacy   *Redacted for Privacy*

Abstract approved _____   〰〰〰〰〰

Dr. John Nábĕlek and Dr. Gordon E. Ness

High seismic activity occurs along the Caribbean and the North American Plate boundary beneath the eastern part of Hispaniola. A large number of intermediate to deep earthquakes are clustered between the Puerto Rico Trench to the north and the Muertos Trench to the south suggesting the possibility of concurrent subduction from both north and south.

The body wave inversion technique was used to analyze nine earthquakes, the largest teleseismically recorded events since the establishment of WWSSN (World Wide Standardized Seismograph Network) in 1963 in the geographic region between 72° W and 66° W latitude and 16° N and 21° N longitude. Their body-wave magnitude ranges from 5.6 to 6.1. Each event was inverted for strike, dip and slip

of the two possible fault planes, as well as for the centroid depth, the total seismic moment and the source time function.

In order to optimize the crustal structure parameters used in the body wave inversion method, a two-dimensional geophysical cross-section across Hispaniola was constructed by forward modeling of gravity and magnetics data.

The inversion results are consistent and can be divided into groups according to the depth and the epicentral location of the events. The shallow events, with depths of 6 to 12 km, represent crustal deformation and show thrust mechanisms with large strike-slip component. The intermediate depth events range from 42 to 107 km in depth and occur to the south of eastern Hispaniola. They show clear thrust mechanisms with a consistent dip of the compressional P-axis at about 30° to the north and approximately north-south P-axis strike. The deep earthquakes occur between 110 and 177 km depth, have a steep-dipping tensional T-axis, and define another slab, possibly originating at the Puerto Rico Trench to the north. One m_b=6.1 event, which occurred on 6/24/84, shows opposite orientations of the P- and T-axes from the surrounding intermediate events. It is interpreted as an interface event in the upper mantle.

The southern subduction zone is well defined and indicates that the Muertos Trench is active, with the subducting plate dipping to the north beneath eastern Hispaniola. At a depth of about 110 km, the northward dipping slab collides with the almost vertical segment of the

other slab. This deep vertical slab segment, extending to at least 200 km in depth, may be a remnant of an earlier subduction zone associated with the Puerto Rico Trench. Alternatively, it may be connected with a more gently dipping part of the slab towards the north or, even in some way, with subduction from the south.

Double Subduction beneath Hispaniola ? An Investigation of

Earthquakes by Body Wave Inversion

by

Rainer Ludwig

A THESIS

submitted to

Oregon State University

in partial fulfillment of
the requirements for the
degree of

Master of Science

Completed November 3, 1989

Commencement June 1990

APPROVED:

Redacted for Privacy

Co-Major-Professor: Assistant Professor of Geophysics

Redacted for Privacy

Co-Major-Professor: Research Associate of Geophysics

Redacted for Privacy

Dean of College of Oceanography

Redacted for Privacy

Dean of Graduate School

Date thesis is presented November 3, 1989

Typed by the author Rainer Ludwig

ACKNOLEDGMENTS

I would like to thank both my major professors, John Nábělek and Gordon Ness, for the opportunity to work on this project. John taught me seismology, and I appreciated that he always found the time to help and advise me. His humor and friendliness are unique among all the professors that I encountered at this university and back home at the Universität Karlsruhe. Gordon taught me plate tectonics and that geophysics is not complete without geology. We had many fruitful discussions not only about science but also about history and politics, which I enjoyed a lot since those topics tend to have lower priority in the United States than in my country.

My thanks are extended to the Geophysics faculty, especially Dick Couch, who advised me on my gravity project, and to Shaul Levi, who helped me when I needed another committee member.

I also appreciated being part of CONMAR: its staff and facilities were a very nice environment for a student. Particularly I want to thank Steve Troseth for doing artistic work to create "page 4" and for sharing his talent on how to present scientific results graphically.

It was very enjoyable being part of an international student body in the Geophysics department. I found friends from all over the world, which made me realize that cultural differences are here to explore and never to look down on. Thanks to Jochen, Haraldur, Daniel, Juan, Ana,

Soofi, Pordur, Luis, John, and all the others. Tim, I will always remember the great ski trips we had.

My special thanks go to my dear friend, roommate, and fellow student Pierre. Without him I would still fear the use of computers instead of having fun with them. We explored this fascinating part of the world, the Pacific Northwest, on numerous trips and his company was always a pleasure. Long live a united Europe!

I want to thank Andrea. With her I did most of my travels and she gave me love and support during my entire university studies. I wish you the best.

Last, but certainly not least, I express my deepest thanks to my family – my mother father and sister. Their love, support, and belief helped me to make the three years in Oregon very enjoyable. I know that they will never forget those few weeks we spent together here in the Wild West. Especially during times of illness it was hard to be so far away. I dedicate this thesis to my father.

TABLE OF CONTENTS

LIST OF FIGURES

LIST OF TABLES

DOUBLE SUBDUCTION BENEATH

HISPANIOLA ?

AN INVESTIGATION OF EARTHQUAKES

BY BODY WAVE INVERSION

INTRODUCTION

The Caribbean Plate is bordered by the North American Plate to the north and east, the South American Plate to the south and the Cocos and Nazca Plates to the west and southwest. The tectonic setting and exact location of the northern part of the Caribbean–North American Plate boundary is very complex and not completely understood.

Figure 1 shows the northern Caribbean region and its general bathymetric features. The bathymetry data were compiled from the "Bathymetry of the Gulf of Mexico and the Caribbean Sea" by Perry (1984) and, in particular around the island of Hispaniola, comprised of the present countries of Haiti and the Dominican Republic, from a marine geophysical survey conducted by Oregon State University in 1986 (Ludwig et al., 1988). One thousand meter contours as well as the

200 m shallow water contour are shown. Names of the larger islands and major tectonic features are given.

Figure 2 is a seismo-tectonic map of the same region. It shows the distribution of earthquakes with body wave magnitudes larger than 4.6 that occurred in the northern Caribbean region between 1963 and 1986. I compiled *Preliminary Determination of Epicenters* (PDE) data for the geographical range of 15° to 22° N and 60° to 90° W. The center of the circle represents the reported epicenter location. The size and grey-shade indicate body wave magnitude and depth ranges according to the legend of Figure 2. Deeper events are overlain by shallower events. High seismic activity is concentrated in the eastern Hispaniola area.

Since plate motion models predict a dominantly strike-slip boundary for this whole region (Minster and Jordan, 1978; DeMets et al., 1989, in press), this untypical seismicity pattern inspired me to conduct a more detailed investigation of recent events beneath eastern Hispaniola.

The purpose of this study is: first to determine the fault mechanisms of the largest teleseismically recorded earthquakes that occurred beneath the Hispaniola area, and second to reexamine the tectonic setting of the area in the light of the seismology results. A reliable method for determining earthquake mechanisms and their depths is the earthquake body wave inversion technique developed by Nábělek (1984), which I used in this project. The method inverts for the source parameters of an earthquake, including the strike, dip and slip of

the fault plane, the centroid depth, the seismic moment and the source time function. It is necessary to have an accurate representation of the crustal structure beneath the epicenters in order to provide credible solutions. This was accomplished by forward modeling of gravity and magnetics data, which were available to me from the 1986 marine geophysical survey. Since earthquakes of interest occurred both onshore and offshore, it was desirable to construct at least two crustal models for the area.
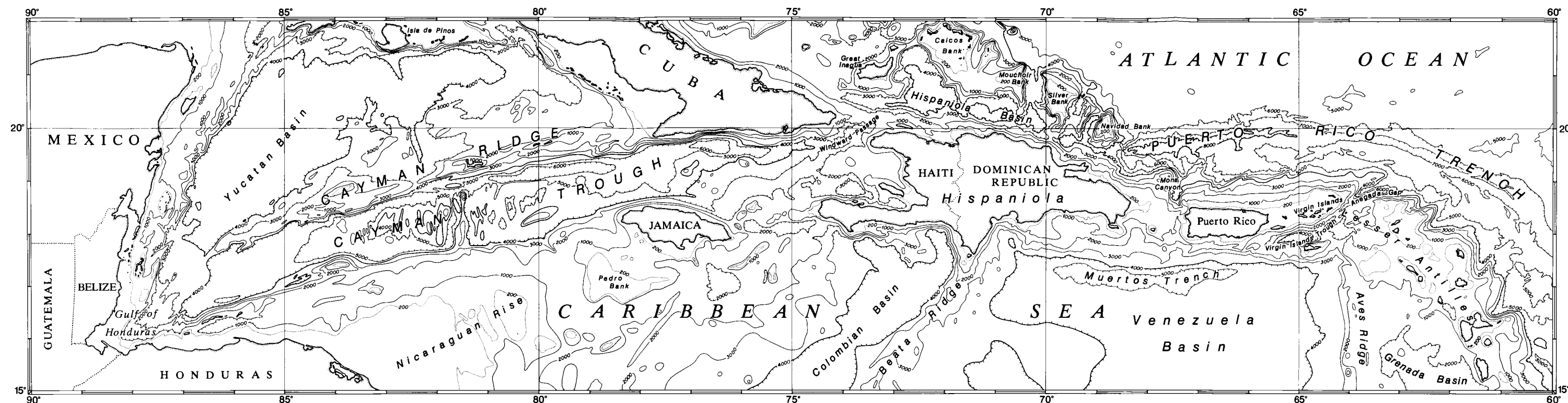
Figure1. Bathymetric map of the northern Caribbean region (contour interval: 1000 m; 200 m dotted)
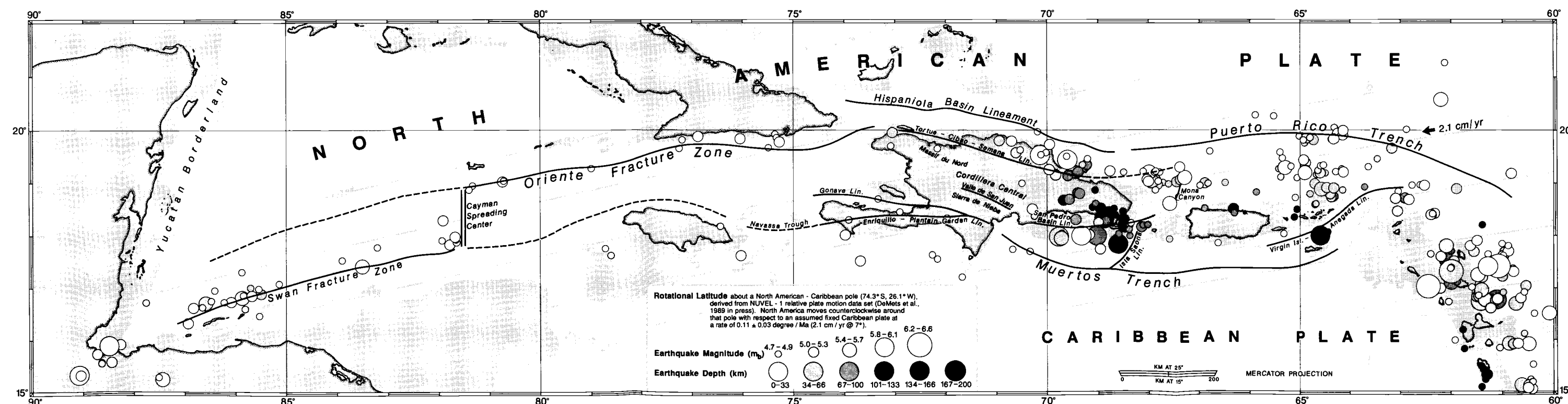
Figure 2. Seismo-tectonic map of the northern Caribbean region

TECTONIC SETTING

Hispaniola is located about 900 km east of the Cayman spreading center (Figure 1) on the northern Caribbean – North American Plate boundary. This spreading center, the only one on the Caribbean Plate, is marked by a cluster of shallow earthquakes (Figure 2). The seismically active lineaments that bound the Cayman spreading center are the Swan Fracture Zone to the southwest and the Oriente Fracture Zone to the northeast (Molnar and Sykes 1969).

The eastern boundary of the Caribbean–North American Plate boundary is characterized by the well studied subduction zone east of the Lesser Antilles Arc (McCann and Sykes, 1984; Tomblin, 1975), which is shown in the southeast corner of the map. Deep earthquakes (more than 200 km) occur just beneath the island arc, while shallow events are located to the east where the bathymetry is deepest.

Structural trends converge onto Hispaniola (Figure 1 and 2). These include the Puerto Rico Trench in the northeast, the Hispaniola Basin in the north, the Oriente Fracture Zone and the Cayman Trough (Holcombe et al., 1973; Wadge and Burke, 1983) in the west, the Nicaragua Rise in the southwest (Shepherd and Aspinall, 1980), the Colombia Basin and the Beata Ridge in the south, and the Muertos Trench in the southeast. Seismic refraction studies (Ewing et al. 1960)

and gravity modeling (Bowin, 1975; Ludwig et al., 1988) revealed that the deep-sea crustal thickness offshore Hispaniola is abnormally thick. The mantle lies 10 to 15 km beneath the seafloor, compared with approximately 6 km for average oceanic crust. In Figure 2, the 1000 m water depth contour is outlined to demonstrate the "continental" character of much of the northern Caribbean region. On the island itself continental crustal rocks are exposed (Bowin, 1975) and gravity data suggest an intermediate depth for the Mohorovicic discontinuity of about 25 km.

A good understanding of the tectonic provinces and features is important for successful crustal structure modeling. Therefore a more detailed description of the tectonic setting of Hispaniola is presented in the following paragraphs. Most of the geologic names that are mentioned in the text can be identified on Figure 1 and Figure 2.

Hispaniola is characterized by approximately west-northwest striking lineaments (Case and Holcombe, 1980). In Figure 2, precisely navigated gravity and bathymetry data were used to outline these lineaments. Very distinct negative free-air gravity anomalies are aligned along an axis north of Hispaniola called the Hispaniola Basin Lineament (Mann and Burke, 1984). Further east this lineament continues as the Puerto Rico Trench (Perfit et al., 1980), a very prominent feature, having water depths of more than 8000 m just east of Hispaniola and showing the largest negative free-air gravity anomalies on earth.

Across the northern part of Hispaniola lies the Tortue-Cibao-Semana lineament (Bowin, 1975; Saunders et al., 1980), a 50 km wide and more than 300 km long landward continuation of the Oriente fracture zone (Case and Holcombe, 1980). It consists of active through-going left-lateral strike-slip faults and vary in strike from 90° to 115° (Mann et al., 1984).

The central part of the island is characterized by reverse, left-lateral or oblique-slip faults (Mann et al., 1984) and consists of alternating valleys and mountain ranges such as the Massif Du Nord in Haiti and the Cordillera Central in the Dominican Republic. These achieve heights of up to 3000 m and include the highest mountain peaks in the Caribbean. Cretaceous through Eocene carbonate rocks are found in the cores of the mountain ranges, typically at elevations higher than 1000 m, while the valleys expose thick sequences of Tertiary and Quaternary sedimentary rocks (Bowin, 1975).

The west and central parts of the island consist of en echelon mountain ranges bounded by dominantly northwesterly trending reverse faults which occur along the edges of the uplifted structures generally near the 500 m topographic contour (Mann et al., 1984). Eastern Hispaniola is much lower than the rest of the island and does not seem to be affected by active surface faulting. Most of eastern Hispaniola is covered by Neogene marine shelf sediments (Bowin, 1975) which show limited regional uplift.

In southern Hispaniola, the Enriquillo Graben is the westward continuation of the Muertos Trench. This fault zone extends west to Jamaica and may merge with the southern edge of the Cayman Trough. The entire lineament has been named the Enriquillo-Plantain Garden Fault Zone (Mann et al., 1984). In southeastern Haiti and in the south-central Dominican Republic, the Enriquillo-Plantain Garden Fault Zone is a straight and narrow zone of deformation that trends due east. However, there is no continuation into eastern Hispaniola where seismicity is more pronounced, indicating that these events must not be associated with surface faults. Southeast of Hispaniola the gravity data show a north-south trending feature called the Isla Saona lineament .

Two models have been proposed to represent present-day plate motions between the Caribbean Plate and its surrounding plates. Jordan (1975) describes the Caribbean Plate as being nearly fixed to a hotspot frame. He inferred relatively slow eastward motion of 2 cm/year based upon spreading rate determinations from magnetic anomalies at the Cayman spreading center and from the disposition of fracture zones. His best-fitting Caribbean–North American pole is located at $50°$ N ± $18°$, $116°$ E ± $9°$ and the computed angular rate is $0.20°$ ± $0.07°$/Ma. These results were used in Minster and Jordan's (1978) plate motion model. The model predicts left-lateral motion along strike-slip faults, predominantly at the northern Caribbean Plate boundary.

A second model, by Sykes et al. (1982) is based on the configuration of the Wadati-Benioff zone at the Lesser Antilles Arc and

the determination of the direction and rate of movement of the Caribbean Plate with respect to North America from slip vectors of shallow earthquakes. This model predicts a convergence rate of approximately 4 cm/year and indicates a best-fitting Caribbean–North American pole near 66° N, 132° W, at an angular velocity of 0.36°/Ma. Hence, there is an azimuthal difference of 25° (anti-clockwise) when compared with Jordan's model. Sykes' model also predicts oblique divergence between the South American and the Caribbean Plate in contradiction with the oblique convergence suggested by Jordan's model. Using the NUVEL-1 data set, Stein et al. (1988) argued that the Jordan geometry provides a better fit to the direction of North America–Caribbean motion.

In Figure 2, flow lines of rotational latitude about the NUVEL-1 Euler pole for the North American and Caribbean Plate pair, which lies at 74.3° S and 26.1° W (DeMets et al., 1989, in press) are shown. The plate motion rate given by NUVEL-1 is 0.11° ± 0.03°/Ma, which is equivalent to 2.07 ± 0.56 cm/year at 7° northern latitude about that pole. The flow lines follow the principal tectonic structures in the northwestern Caribbean such as the Oriente and the Swan fracture zone. However, the major tectonic features on Hispaniola, like the Enriquillo-Plantain Garden Fault Zone and the Tortue-Cibao-Semana lineament, and even the orientation of the island as a whole are inclined considerably to these predicted lines of plate motion. They show a general trend from west-northwest to east-southeast, instead of west-southwest to east-northeast. These distinctive differences in fault

orientations and the occurrence of intermediate to deep earthquakes beneath eastern Hispaniola indicate that this part of the northern Caribbean is certainly more complicated than a simple strike-slip boundary.

DISTRIBUTION OF SEISMICITY

The *Preliminary Determination of Epicenters* (PDE) program is an earthquake catalog system that was begun in 1937. It is presently conducted by the National Earthquake Information Center, part of the United States Geological Survey. Body wave magnitudes (m_b) have been computed routinely since April 1963. I used 1963 as a lower cutoff date in my work. If hypocenter solutions are poorly constrained, a focal depth of 33 km, the average thickness of the crust, is assigned. Such earthquakes were excluded from Figure 2. PDE data, up to October 1986, were available to me on computer tape.

Figure 3 illustrates the body wave magnitude distribution of the earthquakes reported by PDE in the geographic area of Figure 1 and Figure 2. Since the accuracy of depth and location may be doubtful in the case of lower magnitude earthquakes, and since those should occur in larger number than higher magnitude earthquakes, I used only events with m_b greater than 4.6 for this study. Figure 3 shows that m_b equal to 4.7 corresponds to the maximum number for a body wave magnitude of all reported events. The number of events smaller than 4.7 decreases, indicating fewer station observations and therefore probably fewer well determined focal parameters.
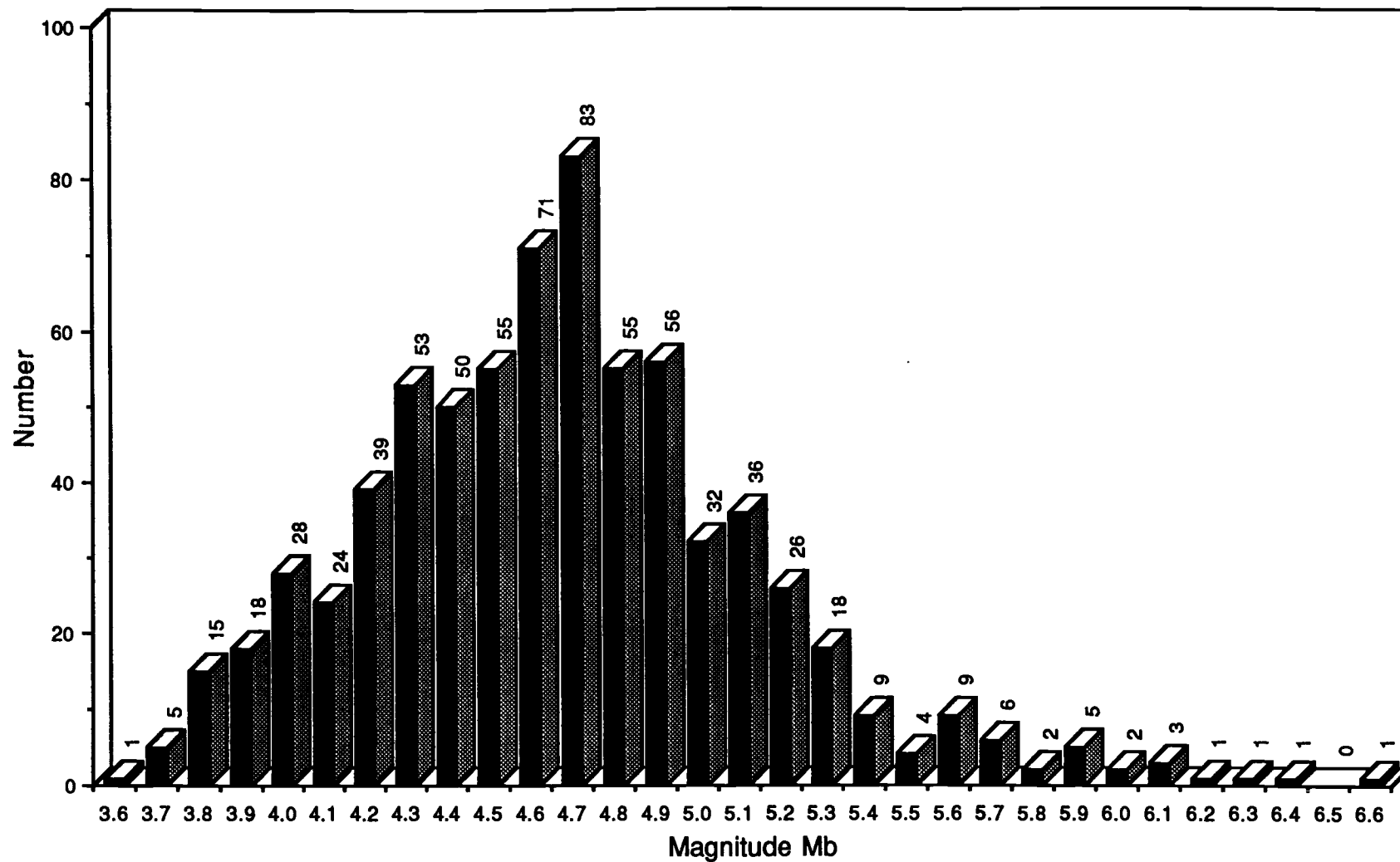
Figure 3. Body wave magnitudes of 709 earthquakes as reported by PDE between 15°N and 22°N and 90°W and 60°W

While there is very little seismic activity within the Caribbean basin itself, the area around Hispaniola is seismically very active. A large number of intermediate to deep earthquakes (up to 200 km deep) occur here. To further demonstrate the depth distribution of earthquakes in that part of the northern Caribbean, I present three vertical seismicity profiles. Figure 4 shows their location. The three different shaded areas represent the range of the selected earthquakes projected onto each section. Each profile is 500 km long. I chose slightly different azimuths for each profile, depending upon the geographical distribution of the epicenters, so that the distances of the epicenters to the line of projection would be minimized.

Figure 5 shows the vertical seismicity profile 1 beneath eastern Hispaniola. Here, as in Figure 6 and Figure 7, the depth reported by PDE is plotted versus the profile length. The southern end of the profile corresponds to 0 km and the northern end to 500 km. Figure 5 includes the events that I studied in detail. These are represented by shaded circles. The position of the Muertos Trench, the Puerto Rico Trench and the location of the eastern part of Hispaniola crossed by profile 1 are plotted relative to the 500 km line. The position of the two trenches refers to the point on the profile where the bathymetry is deepest.

It is in this relatively narrow zone that the greatest number of earthquakes occurs. Shallow earthquakes appear south of the Muertos Trench at a profile length of approximately 150 km. There appears to be a gap in seismic activity just where the Muertos Trench is deepest.
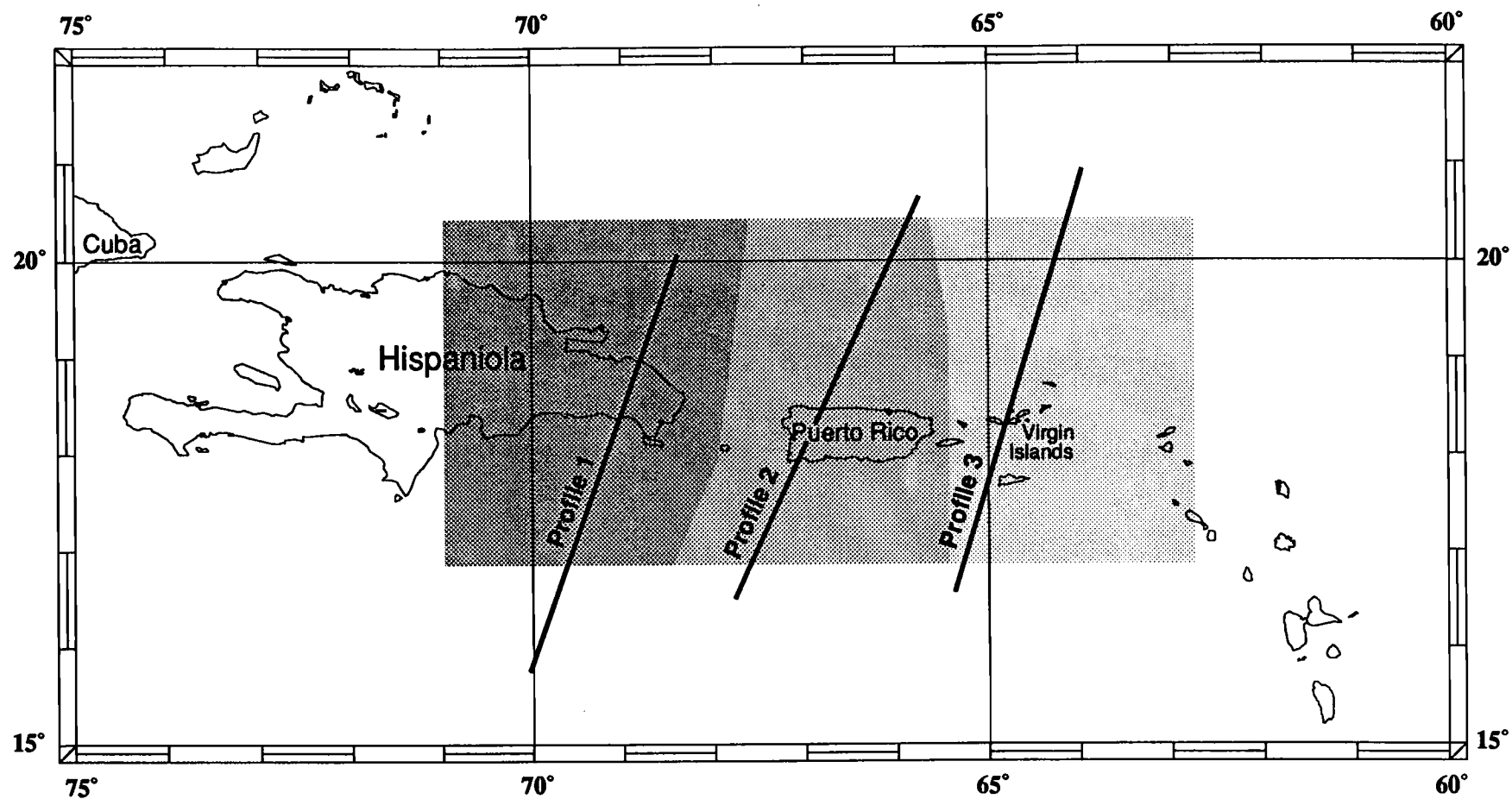
Figure 4. Seismicity profile location map
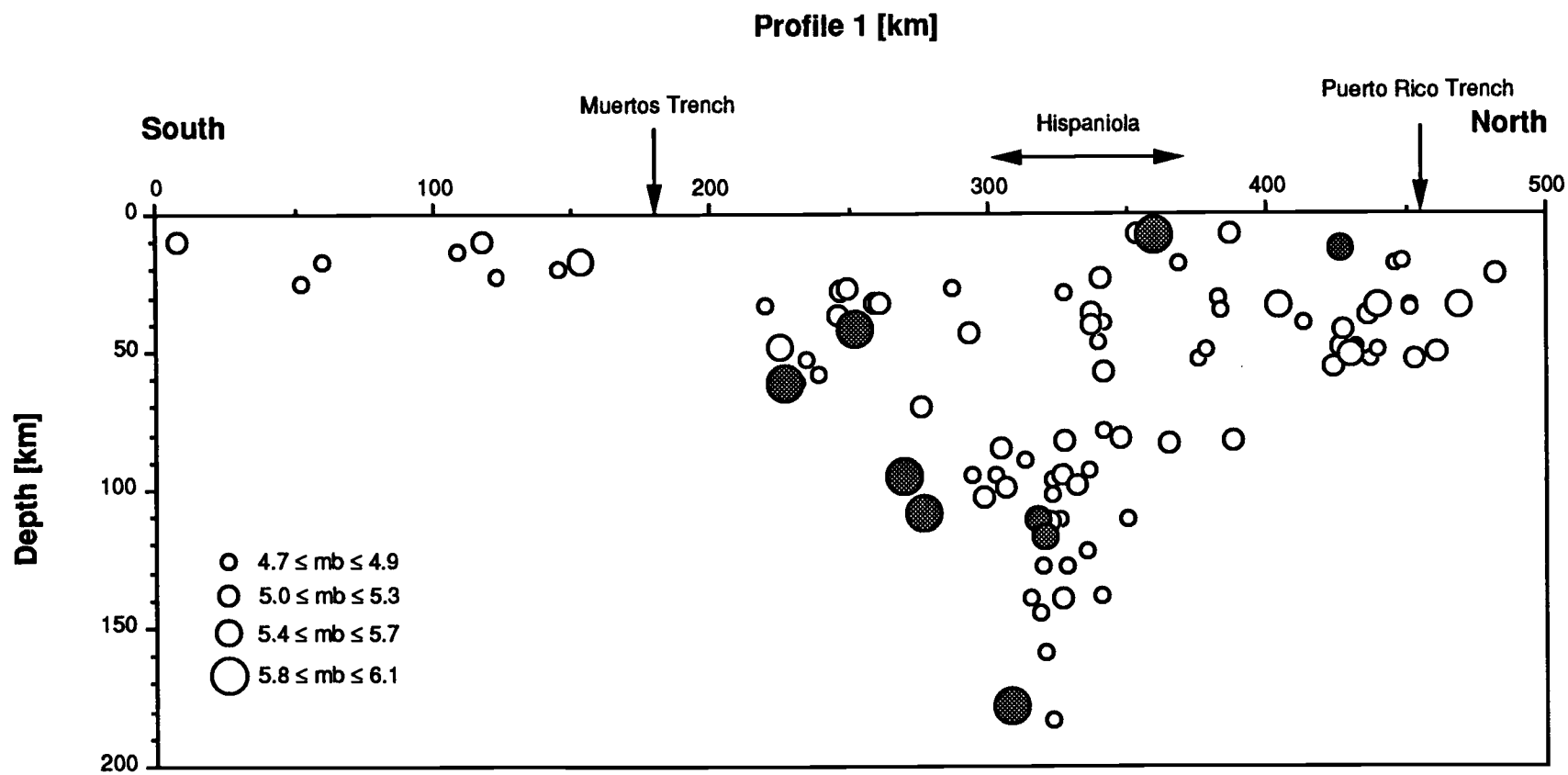
Figure 5. Vertical seismicity profile 1 (azimuth = 20°) beneath eastern Hispaniola;
Studied events are shaded

Further north, earthquakes occur progressively deeper, with maximum depths close to 200 km beneath the southeast tip of Hispaniola. A little further north, still beneath the island of Hispaniola, earthquakes of all depth ranges, from upper crust to depths of 150 km, occur. And at another 50 to 120 km north a cluster of lower crust and upper mantle events is evident.

The overall pattern of seismicity suggests the possibility that a double subduction zone exists beneath the southeast tip of Hispaniola with convergence occurring from both the north and south. Further east this is not the case. Figure 6 shows the vertical seismicity profile beneath Puerto Rico. Earthquakes occur down to about 110 km. Beneath the two positions where the Muertos Trench and the Puerto Rico Trench are deepest, seismic activity is absent. However, shallow events are located beneath Puerto Rico and deeper events occur beneath the northern coast of the island. The data are not conclusive as to whether subduction occurs from the north or the south. The possibility of subduction from both sides cannot be excluded but the seismic pattern is not as striking as that of profile 1.

The seismicity profile beneath the Virgin Islands is shown in Figure 7. In this area, indicated on Figure 4 with the lightest grey-shade, a large number of earthquakes occurs in the upper mantle with a few at depths of 80 to 150 km. Beneath this part of the Puerto Rico Trench a cluster of events in the lower crust to upper mantle is prominent. Further to the south about 50 km north of the Virgin Islands, another cluster of upper mantle earthquakes is visible. Still
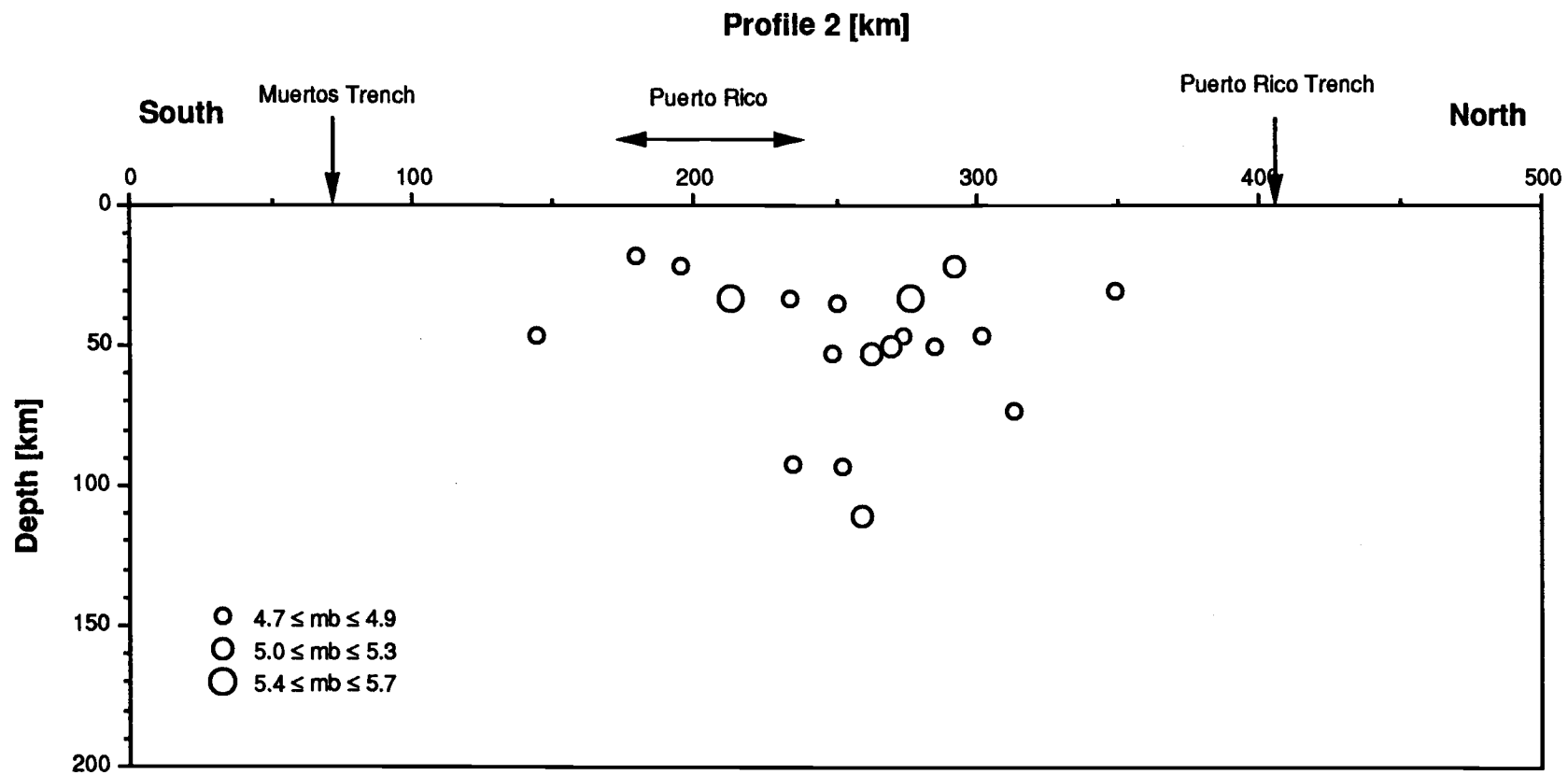
Figure 6. Vertical seismicity profile 2 (azimuth = 25°) beneath western Puerto Rico
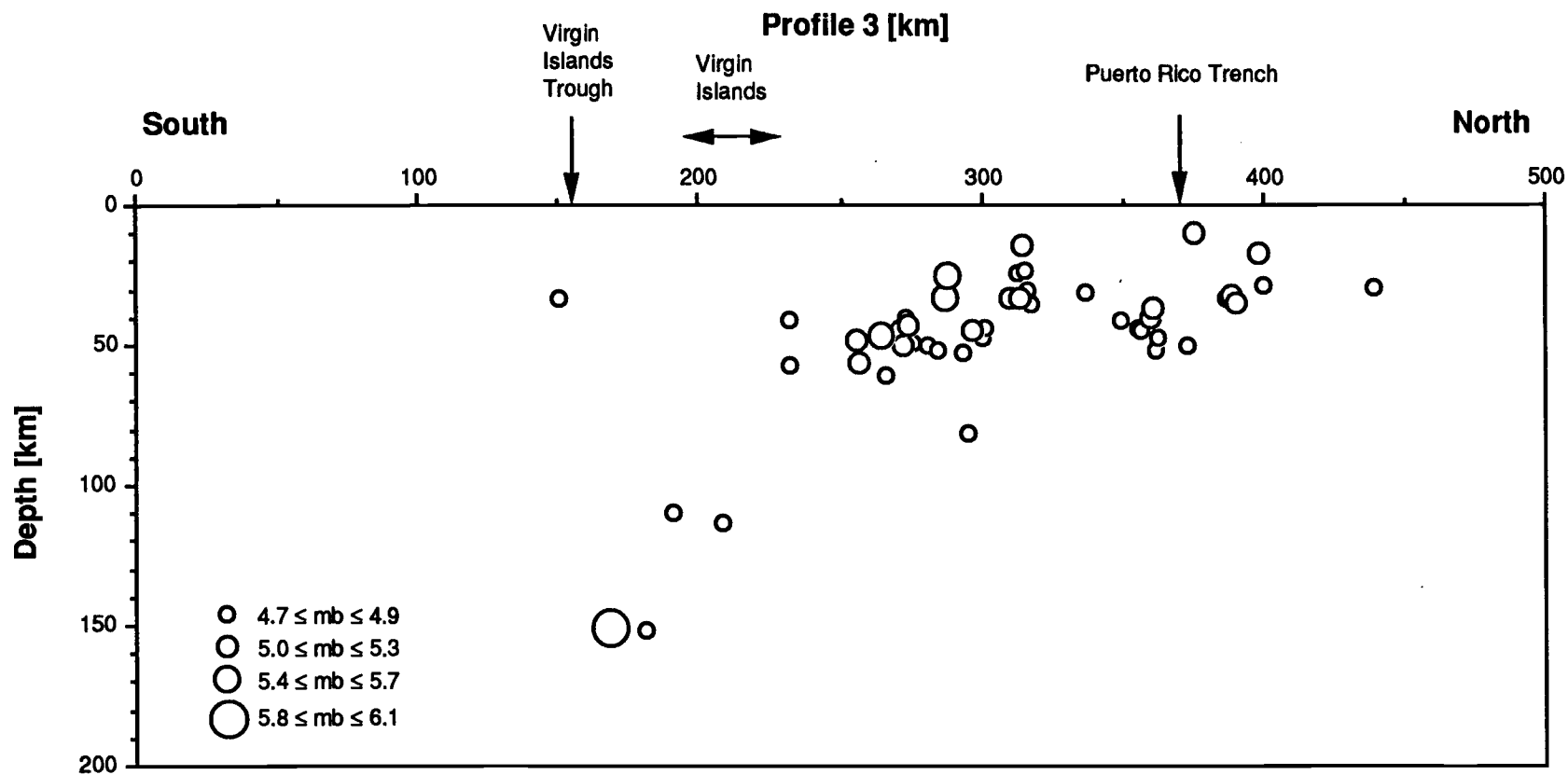
Figure 7. Vertical seismicity profile 3 (azimuth = 17°) beneath the Virgin Islands

further to the south, beneath the southern edge of the Virgin Islands, a few deep events occur. This seismic pattern indicates a slab subducting from the north, originating at the Puerto Rico Trench. There is one relatively shallow event reported in the crust beneath the Virgin Islands Trough, a bathymetric depression and a possible eastward extension of the Muertos Trench, 40 km south of the Virgin Islands.

Another way of showing the seismicity pattern at the Caribbean–North American Plate boundary is presented in Figure 8 and Figure 9. Using the same seismic data that were projected onto Figure 2, I divided the entire data set into 33 kilometer depth increments and plotted six separate layers of depth ranges in map view. The layers have the same geographical bounds as in Figure 4 and have the same magnitude ranges and grey-shade patterns as in Figure 2.

In the Lesser Antilles region, the depth distribution of earthquakes associated with this well studied subduction zone (McCann and Sykes, 1984) describes the downgoing slab of the North American Plate beneath the Caribbean Plate from east to west. Further west, subduction appears to continue north of the Virgin Islands. It seems to be connected with part of the Puerto Rico Trench, and the deepest events occur beneath the Virgin Islands Trough – a bathymetric depression and a possible eastward extension of the Muertos Trench – 40 km south of the Virgin Islands (Figure 1). Between the Dominican Republic and Puerto Rico, beneath the Mona Canyon, a prominent bathymetric feature between eastern Hispaniola and Puerto Rico (Figure 1), an eye-catching cluster of shallow to upper mantle earthquakes
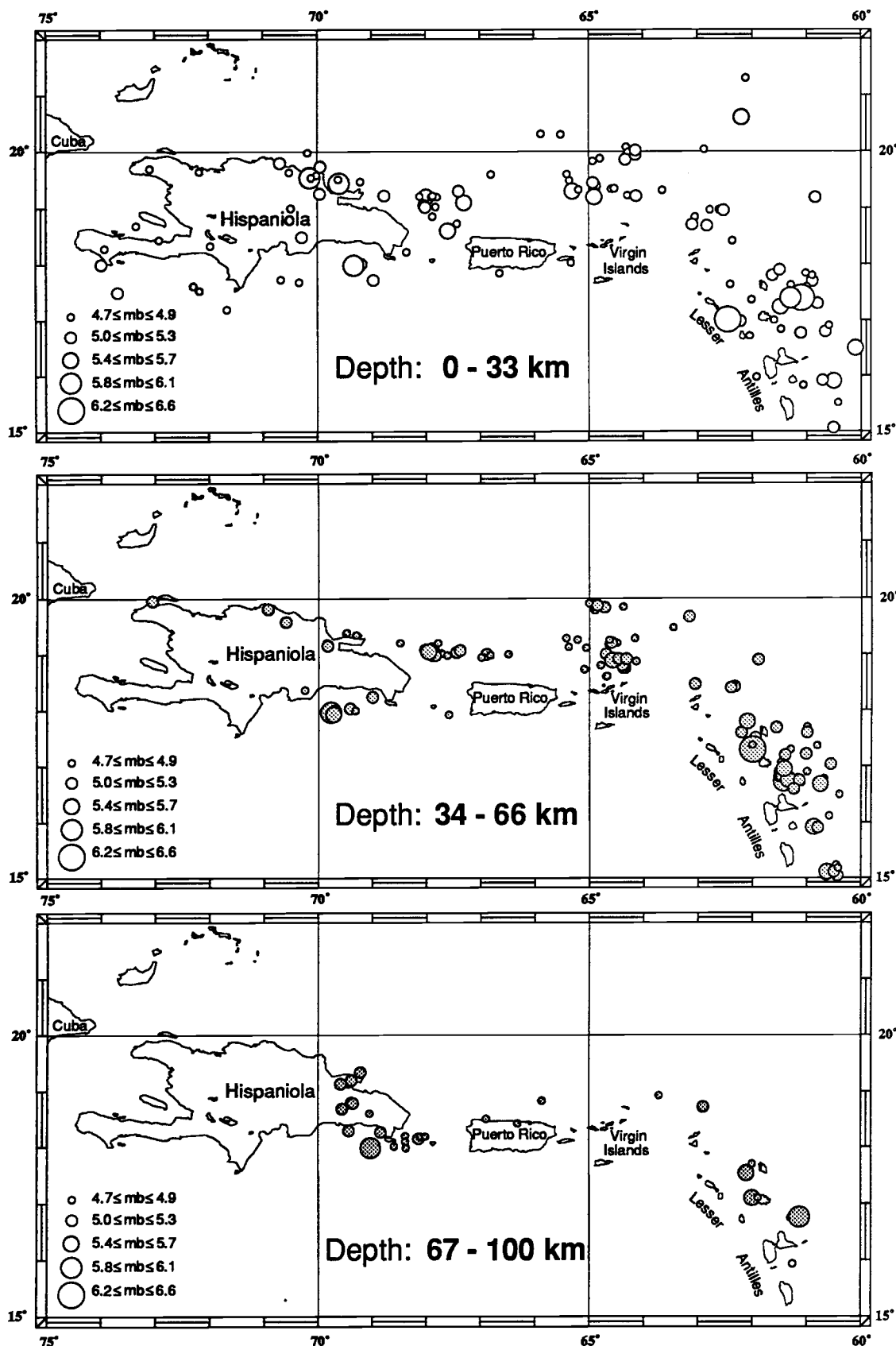
Figure 8. Depth distribution of earthquakes between 0 and 100 km
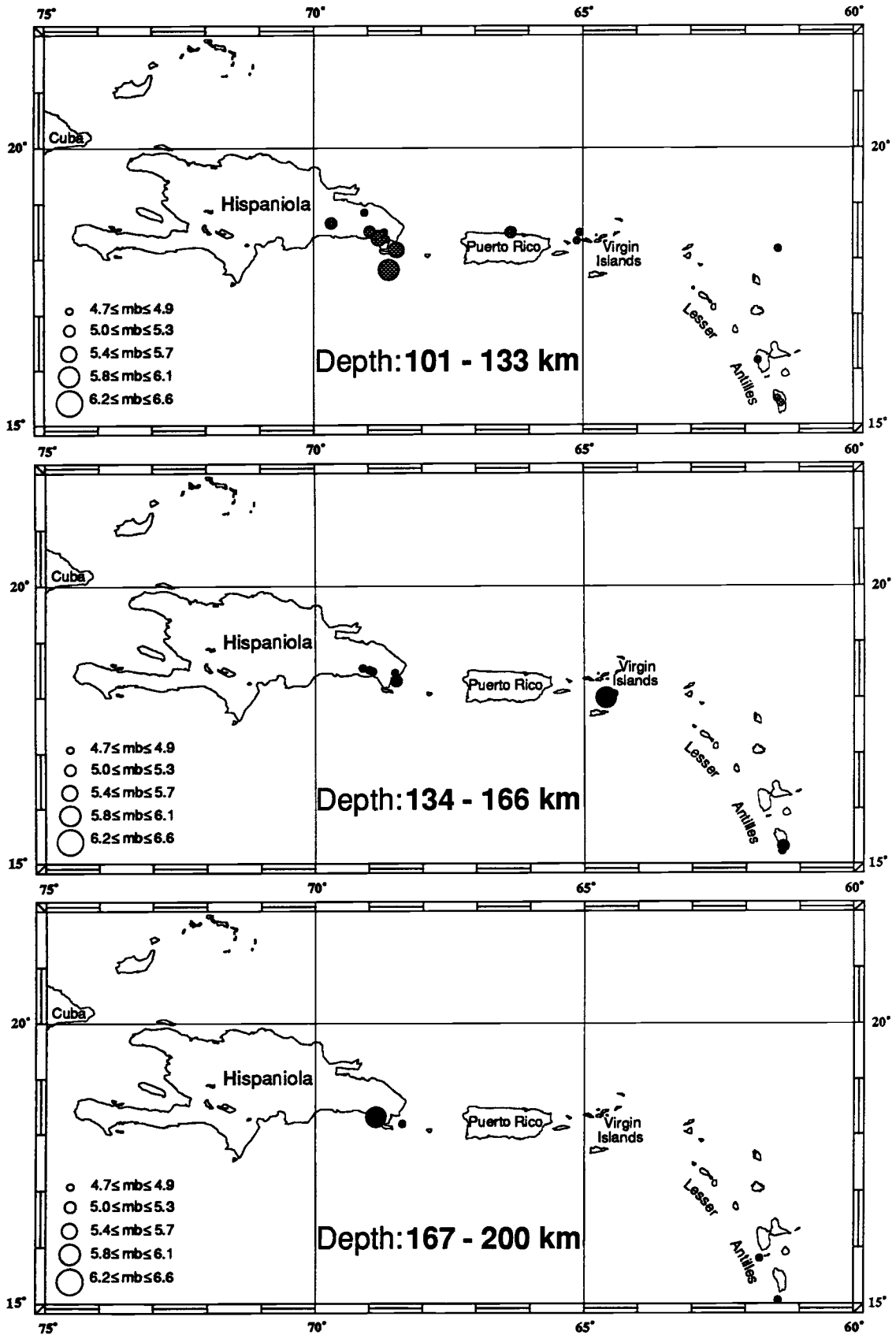
Figure 9. Depth distribution of earthquakes between 101 and 200 km

appears. However, most striking is the seismic pattern beneath the eastern part of Hispaniola.

From this compilation alone, one can not infer that double subduction is indeed occurring. Exact geographic locations, the magnitude range, and especially the focal depth of PDE reported earthquakes can be questionable. Therefore, in order to answer the question of what kind of tectonic interaction those earthquakes represent, a more detailed investigation of several events is necessary. To solve for the mechanism of large magnitude earthquakes, I applied the earthquake body wave inversion technique (Nábělek, 1984). This method inverts for the strike, dip and slip angle of the two possible fault planes, the depth of the centroid, as well as for the total seismic moment and the source time function. The results have a relatively high accuracy providing that an assumed crustal structure is correct. A good estimate of the crustal structure beneath Hispaniola may be obtained by constructing a geophysical cross-section across the island from potential field data. I have constructed such a section and it is discussed in a subsequent chapter.

EVIDENCE FOR SUBDUCTION BENEATH HISPANIOLA FROM PREVIOUS STUDIES

Focal mechanism determinations in the Caribbean region were made by Molnar and Sykes in 1969. Their work first suggested underthrusting beneath eastern Hispaniola from the north. Bracey and Vogt (1970) interpreted Molnar and Sykes' mechanisms as hinge faults, since the fault plane solutions not only show a large component of thrusting but also a component of strike slip movement. Bracey and Vogt proposed that those hinge faults terminate a small slab of the North American Plate underthrusting the eastern part of Hispaniola from both the north and the south.

Bowin (1975) pointed out that most earthquake activity between 1900 and 1973 is east of 70 ° 30' W and that a cluster of intermediate-depth earthquakes occurs in the vicinity of eastern Hispaniola. He also mentioned that a few earthquakes just south of eastern Hispaniola had hypocenter depths greater than 150 km, possibly related to subduction from the north.

Ladd et al. (1977) studied multi-channel seismic reflection records over the Muertos Trench south of eastern Hispaniola. They interpreted the Muertos Trench as being the boundary between the overriding Greater Antilles Island Arc and subducting Venezuela Basin

crust to the south. The seismic records show evidence for underthrusting beneath an accreted sediment wedge against the margin of the basin, typical of convergent margins.

Biju-Duval et al. (1982) further interpreted the reflection seismic records mentioned above. They identified several structural features including an accretionary wedge and a forearc basin. Geological studies in southeast Hispaniola conducted by Biju-Duval et al. provided further sedimentologic and stratigraphic evidence for active subduction from the south.

Byrne et al. (1985) studied a large event that occurred on the 24th of June in 1984 south of Hispaniola beneath the Muertos Trench. They suggest that the mechanism of that earthquake, obtained from body wave inversion, together with results from other unspecified events, indicates active thrusting between the Caribbean Plate and the southern coast of Hispaniola and a compressional deformation of the subducted Caribbean Plate. I reanalyzed this event inverting for more P and SH waves than did Byrne et al. Additionally, their solution was achieved using a half-space, one-layer crustal model. My solutions were attained using a more realistic crustal model. However, for comparison, I also inverted the body wave data with the half-space crustal model. The results are discussed later.

Stephan et al. (1986) stated that both the Puerto Rico Trench and the Muertos Trench mime subduction zones orientated perpendicular to the Lesser Antilles Arc. Due to the lack of volcanism, and their claim that

characteristic seismicity is missing, Stephan et al. proposed to call these structures "pseudosubductions".

Recently Dillon et al. (1989, in press) described an accretionary wedge north of Haiti and the westernmost Dominican Republic, indicating thrusting beneath Northern Hispaniola from the north. Long-range sidescan sonar, multichannel and single channel seismic reflection profiles provided data for this study. Two different slopes were obtained for the shallow part of the subducting slab: a gentle slope north of Haiti dipping 4°, and a steeper slope of 9° to 16° further to the east.

POTENTIAL FIELD DATA AND CRUSTAL CROSS-SECTION

In 1986 CONMAR, the *Continental Margins* Study Group at Oregon State University, in cooperation with the Instituto Cartografico Militar of the Dominican Republic conducted, a marine geophysical survey (Hispaniola 86) around the island of Hispaniola. Bathymetric, gravimetric and magnetic data were sampled along 15,500 km of tracklines onboard the Mexican Navy ship "Altair". The trackline spacing north of Hispaniola was approximately 4 nautical miles and about 5 nautical miles south of the island (Ludwig et al., 1988). The data sample spacing along track was 0.14 nautical miles for navigation, bathymetry and magnetics and 0.42 nautical miles for gravity data.

Bathymetric data were obtained using an echo sounder and analog records were later digitized at 1 minute distance intervals. The recorded two-way travel times were converted into depths in corrected meters. The bathymetric data quality which is represented by the root-mean-square (rms) mistie for trackline crossings was 47.5 m in the northern portion and 52.3 m in the southern portion of the survey, reflecting the extremely steep gradient in the survey area. For the compilation of the bathymetric map (Figure 1), these data were included around the

Hispaniola area, in the geographical region of 16.5° to 21.5 ° N, and 67° to 75° W.

After standard corrections were applied to the gravity data, the free-air anomaly was computed. The root mean square trackline crossing discrepancy was 1.71 mGals (125 track crossings) in the very accurately navigated northern portion of the survey and 2.94 mGal (62 track crossings) south of Hispaniola. This high-quality data set was available to me in a grid format with one km spacing. Additionally, I modeled marine magnetics data that were digitally sampled north of Hispaniola during the same cruise. An rms crossing discrepancy of 19.5 gammas, uncorrected for diurnal variation, was calculated for the entire survey.

In order to get a reasonable estimate of the crustal structure beneath the island of Hispaniola, I used constraints from seismic refraction, gravity, magnetic and bathymetric data to construct a crustal and upper mantle modeled cross-section over the island of Hispaniola.

Figure 10 shows the location of the cross-section, which was chosen to satisfy the two-dimensionality required by the forward modeling program developed by Talwani et al. (1959). The approximate northeast-southwest orientation is nearly perpendicular to the direction of the mountain ranges, valleys and major faults on Hispaniola and the associated long axis of the principal gravity and magnetic anomalies. In addition, the location of the profile was selected so the model could be tied to a seismic refraction line obtained by
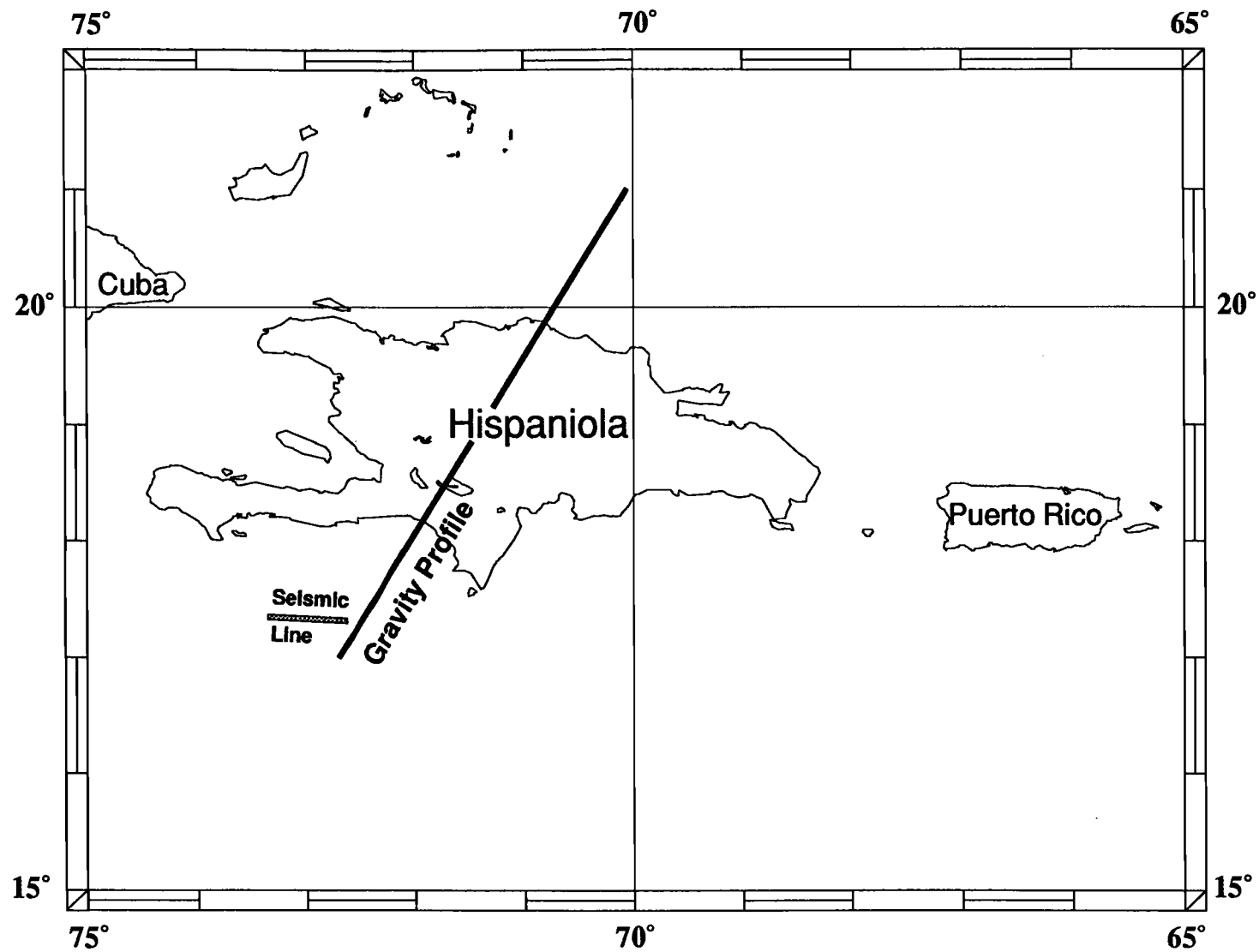
Figure 10. Location of geophysical cross-section across Hispaniola and seismic refraction line

Ewing et al. (1960). This line was shot west to east, just south of Haiti and west of the Beata Ridge. Five layers were found with seismic velocities of 2.0, 3.6, 4.9, 6.1 and 7.8 km/s. The location of the refraction profile is shown on Figure 10. Seismic velocities were converted into layer densities using the empirical relation of Ludwig et al. (1970).

A model of the crustal and upper mantle structure was constructed, assuming that no lateral inhomogeneities exist in the mantle below 50 km. Water depths were obtained from the bathymetric data described above. Topographic values onshore were digitized from regional maps. Using the line integral method developed by Talwani et al. (1959), the vertical component of the gravitational acceleration was computed along the profile as being the sum of the gravitational accelerations caused by two-dimensional mass polygons representing the different layers. The results yielded the gravitational acceleration along the profile produced by the model. The free-air gravity anomaly was then computed by subtracting 6442 mGal from the total gravitational acceleration. This is the value computed by Barday (1974) for an average oceanic section 50 km thick, assuming a zero free-air anomaly. Artificial mass columns were used to tie the section at the northeast and southwest ends to standard oceanic mass columns, in order to prevent unreal edge effects at the ends of the section.

Iterative adjustments during forward modeling of the shapes of the polygons and of their corresponding densities, yielded calculated

free-air gravity anomalies approaching the observed anomalies. As an additional constraint, magnetic data were used in the northern part of the geophysical cross section. The magnetic anomalies were computed using the method of Talwani and Heirtzler (1964), and take into account the local inclination and declination of the regional field. The values obtained were then normalized to the observed anomalies by subtracting from all computed anomalies the difference between the theoretical and observed magnetic anomaly at the first station.

The final model includes all constraints and is presented in Figure 11. The circles in the upper part of Figure 11 represent observed gravity values and the continuous line portrays the computed free-air anomalies. A data gap exists onshore near the profile length of 200 km. The overall fit is good, with calculated free-air anomalies matching observed values at each station to within a few mGals. In the lower part of Figure 11, depth is plotted versus profile length with a vertical exaggeration of about 3:1. South of Hispaniola, the layering of the seismic refraction line was used for the model, while the marine northern part incorporated a magnetic layer computed to fit the observed magnetic data, as mentioned above. Due to lack of constraints the onshore segment of the cross section was modeled using a standard continental layering described by Barday (1974). The small blocks on top represent slightly different density values on the surface due to outcrops of various geologic features along the profile, including plutonic and volcanic rocks, metamorphic rocks, and sedimentary rocks
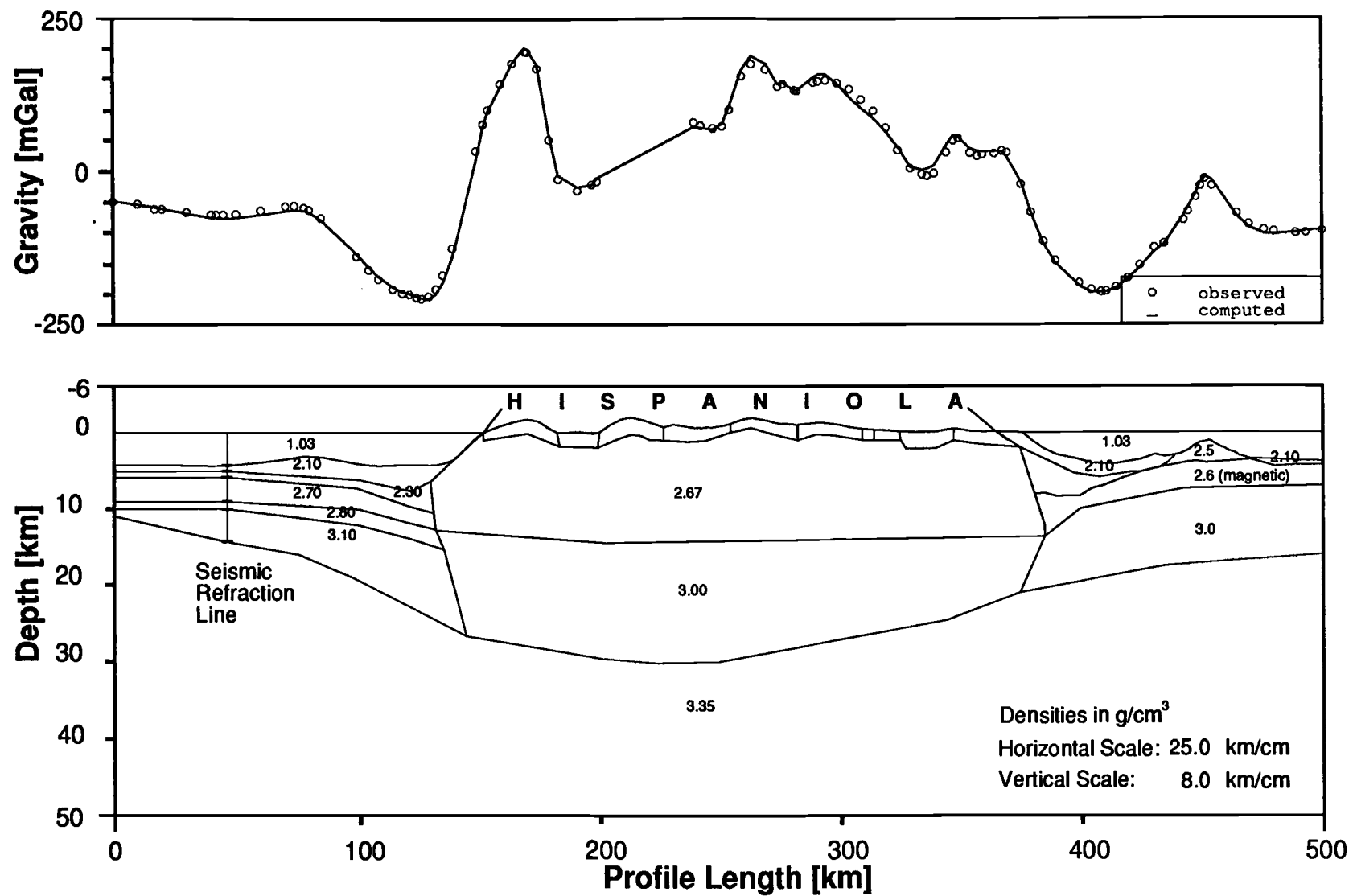
Figure 11. Two-dimensional geophysical cross-section across Hispaniola

from lower Cretaceous to upper Quaternary age (Case and Holcombe, 1980).

The model provides a reasonable estimate of the crustal structure around Hispaniola. As mentioned earlier, the continental crustal character of the island of Hispaniola is confirmed by the depth (up to 30 km) to the Mohorovicic discontinuity. The crustal thickness offshore is abnormally large, with about 17 km to the Moho, despite water depths of more than 4000 m, which is typical for old oceanic crust.

The results of this crustal cross-section provided an input for the waveform inversion. Two crustal models, one for the events occurring offshore and one for those earthquakes having hypocenters beneath the island itself, were used.

THE BODY WAVE INVERSION METHOD

The theory behind the body wave inversion technique is described by Nábělek (1984). At teleseismic distances P and S waves are sufficiently separated in time from each other and from other seismic phases so that they can be analyzed independently. The source mechanisms of the earthquakes are determined by matching waveform and amplitude of synthetic seismograms for both P and S waves to observed long-period seismograms in a least squares sense.

The body wave inversion technique inverts for the source centroidal parameters. These are the double-couple orientation of the earthquake in strike, dip and slip angle (using the convention by Aki and Richards, 1980), the centroidal depth (an average depth along the rupture), the far-field source time function, parameterized by a series of isosceles triangle functions with adjustable relative amplitudes and durations, and the scalar seismic moment, representing the source strength. If there is no serious noise contamination and if long-period teleseismic body wave data of azimuthally well-distributed stations are used, the P wave packet carries sufficient information to determine the basic centroidal parameters of the source (Nábělek, 1984). The additional use of S wave packets constrains the source parameters further. The accuracy for the centroid depth is about 2 km.

Only long-period seismograms from recording WWSSN (World Wide Standardized Seismograph Network) and from GDSN (Global Digital Seismograph Network) stations at an angular distance range of 30 to 90° were analyzed in this study. These waves propagate steeply through the crust and uppermost mantle, where lateral heterogeneities are greatest.

Figure 12 illustrates the travel path of the teleseismic P and S waves. Assuming a single point source in a layered source region, the synthetic seismograms are computed by a convolution of three effects: the contributions from the crustal and free surface effects of both the source and receiver regions and the contribution from the mantle. The convolution can be expressed as:

$$\underline{g}(t) = \underline{g}^{s}(t) * M(t) * \underline{C}^{r}(t)$$

where $\underline{g}^{s}(t)$ is the displacement of the P, SH or SV waves emerging at the bottom of the crust in the source region in response to an earthquake; $\underline{C}^{r}(t)$ describes the effect of the crust underneath the receiver; $M(t)$ is the response to these waves by the mantle.

To obtain reasonable source parameter estimates it is important to know about the crustal structure in the vicinity of the earthquake hypocenter. Here is where the crustal model that was discussed above is applied. It is from this crustal structure that excitation functions are computed. Primary contributing phases to these excitation functions are
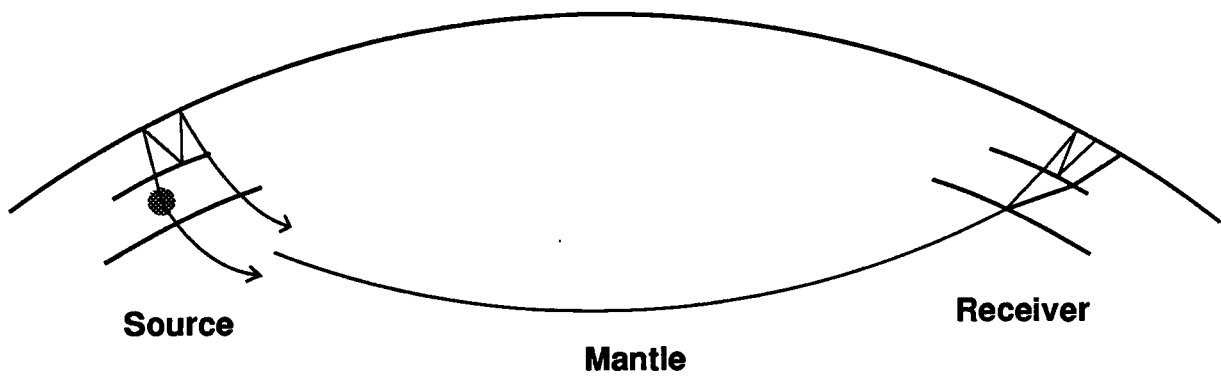
Figure 12. Path of teleseismic P and S waves through crustal structures in the source and receiver region, and attenuation in the mantle

the P, pP and sP phases for the P wave packet, the S and sS for the SH wave packet and the S, pS and sS phases for the SV wave packet. Typical attenuation factors t* (ratio of travel time to average Q) equal to 1 s for P waves and 4 s for S waves were used. Due to to the higher attenuation, S waves lack the high-frequency resolution of P waves.

M(t) has few components due to the mantle's near homogeneity and by the restriction that only receivers at an angular distance range of 30° to 90° are considered. Therefore,

$$M(t) = G * A(t, t^*) * \delta (t - t_m),$$

where G is a geometrical spreading factor, $A(t, t^*)$ represents anelastic attenuation and $\delta (t - t_m)$ expresses the travel time in the mantle. Therefore M(t) does not contribute to the generation of other phases.

No unusual crustal structures in the receiver region are expected, since most of the stations of the WWSSN and GDSN used in this study are located on hard rock. Therefore a common half-space structure was assumed for the receiver sites, so that local effects in the receiver structure can be neglected, since they probably average out.

The unknown source parameters are determined by an iterative procedure that requires an initial guess at the parameters. These can be obtained by determining a fault plane solution using classical first motion techniques. Repeated calculations of the theoretical seismograms lead to a minimization of the root-mean-square error between theoretical and observed seismograms in a least squares sense.

SEISMIC DATA AND THEIR PREPARATION

Seismic data that were either recorded on paper by WWSSN or digitally recorded by GDSN (available for earthquakes with magnitudes m_b larger than 5.5 since 1980) were used in this study. Nine earthquakes that occurred between 1963 and 1985 in the geographic region between 72°W and 66°W and 16°N and 21°N were analyzed using the techniques described above. Table 1 gives the epicenter locations, origin times, number of reporting stations, depths, body wave and surface wave magnitudes (if determined) of those earthquakes as reported by PDE. I used the date of the earthquake occurrence to identify the studied events. The locations of the studied events are shown on Figure 13; I plotted the depth range in the same grey-shade pattern as in Figures 2, 8 and 9. The size of the circles represents the seismic moment.

Long-period seismograms from stations of the WWSSN network at an angular distance range of $30° < \Delta < 90°$ from the epicenter were examined and hand-digitized. In digital form the data were interpolated to equal time intervals of 0.5 s. I tried to assure good azimuthal coverage of the stations whenever possible. Linear trends in the data were removed, and in few cases a high-pass filter with a cutoff of 0.0166 Hz was applied to remove long-period trends. The data from different stations were then normalized to a common instrument

Date [mo/day/yr]	hr/min/sec	Latitude [°]	Longitude [°]	Depth [km]	m_b	M_s	Number of stations
12/22/64	08/01/12.6	18.40	291.20	115	5.6	-	37
06/11/71	12/56/04.3	17.97	290.22	57	6.1	-	132
09/19/72	01/36/52.4	19.54	289.85	33	5.8	6.1	140
03/23/79	19/32/31.1	17.99	290.96	80	6.1	-	356
11/05/79	01/51/12.9	17.83	291.38	104	5.9	-	209
09/14/81	12/44/29.8	18.32	291.11	170	5.9	-	291
09/20/83	08/50/58.3	18.18	291.53	101	5.6	-	242
06/24/84	11/17/11.9	17.98	290.66	24	6.0	6.7	331
07/21/85	13/10/35.0	19.05	292.03	35	5.7	5.3	265

Table 1. PDE data
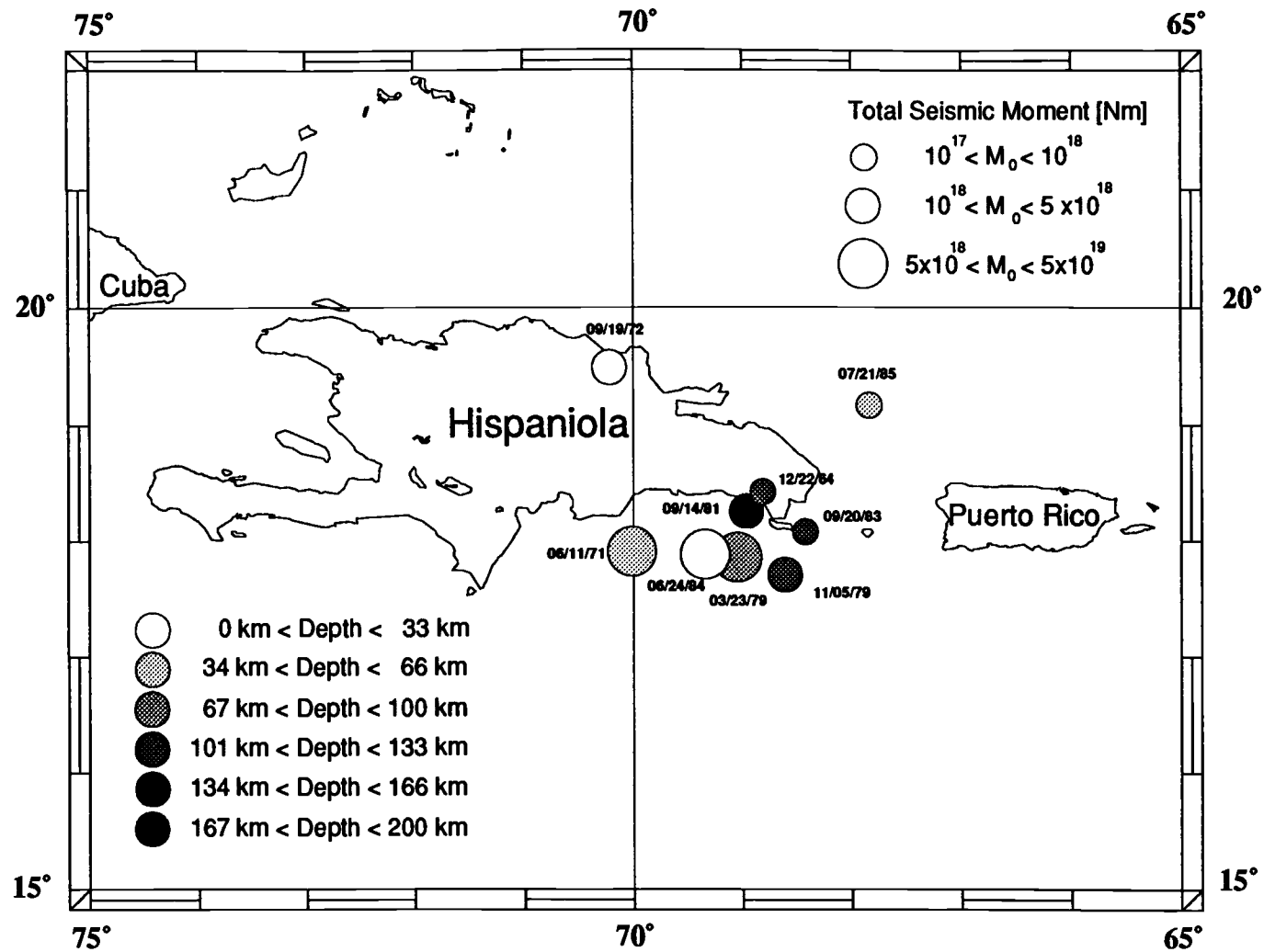
Figure 13. Location map of studied earthquakes

magnification of 1500 and an epicentral distance of 40°. According to the root mean square amplitudes of P and S waves, different weights were applied for different phases (Nábělek, 1984). In addition for some events I assigned different weights for azimuthally uneven distributed stations. This will be discussed in detail for those specific events.

Short-period seismograms were used to determine the P wave arrival time at a given station (typically with an accuracy of 0.5 s) to better constrain the alignment of the observed data and the theoretically computed seismogram. Additionally, short-period and long-period data at a distance range of $0° < \Delta < 90°$ were used to determine first motion directions of the P waves. The first motion determinations were used to provide an initial guess for the body wave inversion. In the Appendix Figures 27, 28 and 29 the first motion polarities are shown on a lower hemisphere projection of the focal sphere.

Digital data from GDSN stations were available for five events that occurred between 1980 and 1985. The time sampling is 1 s for long-period instruments with a peak gain at T = 28 s. The same normalization and filter procedures were applied to the digital data set as to the analog data and both types of seismograms were combined for the inversion.

Two crustal structure models were used for the inversion. They are described in Table 2. The *Island Crustal Structure* was used for the two epicenters that were located on land (Event 12/22/64 and Event 09/19/72). The other events occurred offshore. The water depth at the

epicenter, indicated with d in Table 2 corresponds to an estimated water depth obtained from CONMAR's bathymetry data and is given in Table 3.

Island Crustal Structure

	Thickness	v_p	v_s	density
Layer 1	13 km	6.0 km/s	3.46 km/s	2700 kg/m^3
Layer 2	11 km	7.0 km/s	4.04 km/s	3000 kg/m^3
Layer 3	200 km	8.1 km/s	4.68 km/s	3350 kg/m^3

Offshore Crustal Structure

	Thickness	v_p	v_s	density
Water	d km	1.5 km/s	0.0 km/s	1030 kg/m^3
Layer 2	2 km	4.0 km/s	2.31 km/s	2300 kg/m^3
Layer 3	(7-d) km	6.0 km/s	3.46 km/s	2700 kg/m^3
Layer 4	8 km	7.0 km/s	4.04 km/s	3000 kg/m^3
Layer 5	200 km	8.1 km/s	4.68 km/s	3350 kg/m^3

Table 2. Crustal structures and seismic velocities used in the body wave inversion

Date [mo/day/yr]	Water depth d [m]
12/22/64	0
06/11/71	900
09/19/72	0
03/23/79	1100
11/05/79	1700
09/14/81	400
09/20/83	1100
06/24/84	1600
07/21/85	2900

Table 3. Assigned water depths for studied events

BODY WAVE INVERSION RESULTS

Introduction

The results obtained from the inversion of body waves of the earthquakes listed in Table 1 allow the events to be divided into three groups according to their depth and location: *Deep events, intermediate events* and *shallow events*. The corresponding results are summarized in Tables 3, 4 and 5. For each event the double-couple source mechanisms are presented for both possible fault planes. Along with the strike and dip angle of the nodal plane, the slip angle is given. This defines the motion of the hanging wall relative to the footwall measured counterclockwise from the strike direction on the footwall (Aki and Richards, 1980). The centroid depth, which is relative to the seafloor for offshore events, and the seismic moment are also given. The azimuth and dip angles of the compressional P-axis and the tensional T-axis, which are related to the mechanism, are included in the tables; they are important for the interpretation of the source mechanisms in their entire tectonic setting.

It is important to understand the range of uncertainties of the derived source parameters. Therefore the formal error, one standard deviation σ, is given. These uncertainties reflect ambient and signal-

generated random noise such as microseismic noise, errors in seismograph calibration or in the assumed crustal structure beneath the recording station (Nábělek, 1987). However, the true uncertainties of these source parameters exceed these formal errors due to the exclusion of several bias factors, such as discrepancies between the assumed crustal structure and that of the "real earth" and uncertainties in the assumed time of the observed waveforms' initial motion. Numerical simulations of waveform inversions by Nábělek (1984) have shown that 2σ is a good estimate of the uncertainty in the seismic moment. More realistic uncertainties for the double-couple orientation angles, strike, dip and slip, and for the centroid depth are generally in the range of 5-10 σ. Hence, rules of thumb for these uncertainties are $\pm$ 4° to 10° for the fault strike, $\pm$ 2° to 6° for the fault dip, 4° to 20° for the fault slip, $\pm$ 2 km for centroid depth and $\pm$ 20% for seismic moment.

Tables 4, 5 and 6 present the solutions of the best fitting double-couple point sources. However, for two events, Event 06/11/71 and Event 03/23/79, a single point source was insufficient to match the observed waveforms. For these events two point sources separated in time and space were necessary to adequately describe the waveforms. The body wave inversion results of those events are given in Table 5. Along with the separate mechanisms for the two sub-events, a combined solution obtained from moment tensor summation is presented. The moment tensor summation provides the best method to represent the total rupture process with a single fault plane solution.

Figures 14 to 23 show the focal mechanisms obtained from the body wave inversion and the observed and synthetic seismograms are presented. For each event the P waves and the SH waves are plotted. In addition, SV waves were included in the body wave inversion for Event 11/05/79.

Seismograms from WWSSN and CSN (Canadian Seismograph Network) stations are indicated by superscript "2" and seismograms from Global Digital Seismograph Network (GDSN) stations are indicated by superscript "3". The observed seismograms are displayed by solid lines and the computed synthetics by dotted lines. Time and amplitude axes are shown in the lower right corner of each seismic diagram. The length of the amplitude scale axis is proportional to the indicated length in cm printed to the left depending upon the seismograph station group (WWSSN/CSN(2) or GDSN(3)). The lines that lead from the seismograms into the circle show the location of a station on a lower hemisphere projection of the focal sphere. The direction of the compressional P-axis and the tensional T-axis are plotted with "P" and "T". The source time function is displayed in the lower left corner of each of these figures.

An initial guess for the source parameters was provided by the P wave first arrivals, which are shown in the Appendix Figures 27, 28 and 29 according to the three depth ranges. The fault plane solutions that were obtained by the body wave inversion are also plotted onto those lower hemisphere projections.

Date	Strike [°]	Dip [°]	Slip [°]	Depth [km]	Mo [10^17Nm]	P-azim. [°]	P-dip [°]	T-azim. [°]	T-dip [°]
12/22/64	294.7±1.4	47.1±0.5	79.0±1.5	116.8±0.6	7.2±0.9	32.5	1.6	133.3	81.8
	130.6±1.4	44.0±0.5	101.6±1.5						
09/14/81	262.0±0.9	56.5±0.3	88.8±0.7	177.1±0.2	17.8±0.5	352.8	11.5	167.8	78.4
	84.1±0.9	33.5±0.3	91.8±0.7						
09/20/83	263.0±1.2	49.7±0.5	111.6±1.2	110.4±0.5	1.5±0.8	337.9	2.5	239.3	73.5
	51.5±1.2	44.8±0.5	66.5±1.2						

Table 4. Inversion results for deep events

Deep Events

Three of the events that were analyzed occurred at depths ranging from 110 to 177 km: Event 12/22/64, Event 09/14/81 and Event 09/20/83. These events are the most northern events of those that cluster at the southeast tip of Hispaniola (Figure 13). Their body wave inversion results are presented in Table 4.

Event 12/22/64

Event 12/22/64 is the only one of the deep events below the island. Therefore the *Island Crustal Structure* was applied for the inversion. Since its magnitude was relatively small, only P waves from two stations were of sufficient quality to be used in the inversion. However, four stations provided good SH waves. The focal mechanism obtained is shown on Figure 14.

The first P-arrival of station NNA is emergent due to the close location to one of the nodal planes. It was difficult to obtain a good match for the direct P wave. However, the reflected phases of the synthetic seismograms aligned well with those of the observed. Station LPB had a clear signal and was fit nicely.

The stations used for SH waves had good azimuthal coverage. The theoretical seismograms provided a good fit to the observed. The source time function is simple, with only two time elements of 1.5 s duration. Occurring at about 117 km depth, the mechanism is clearly one of a

12/22/64

P Wave

WWSSN/CSN(2) = 0.162cm

amp

0 10 20 30
Time (s)

SH Wave

Source Time Function

0 1 2 3 4
Time (s)

WWSSN/CSN(2) = 0.344cm
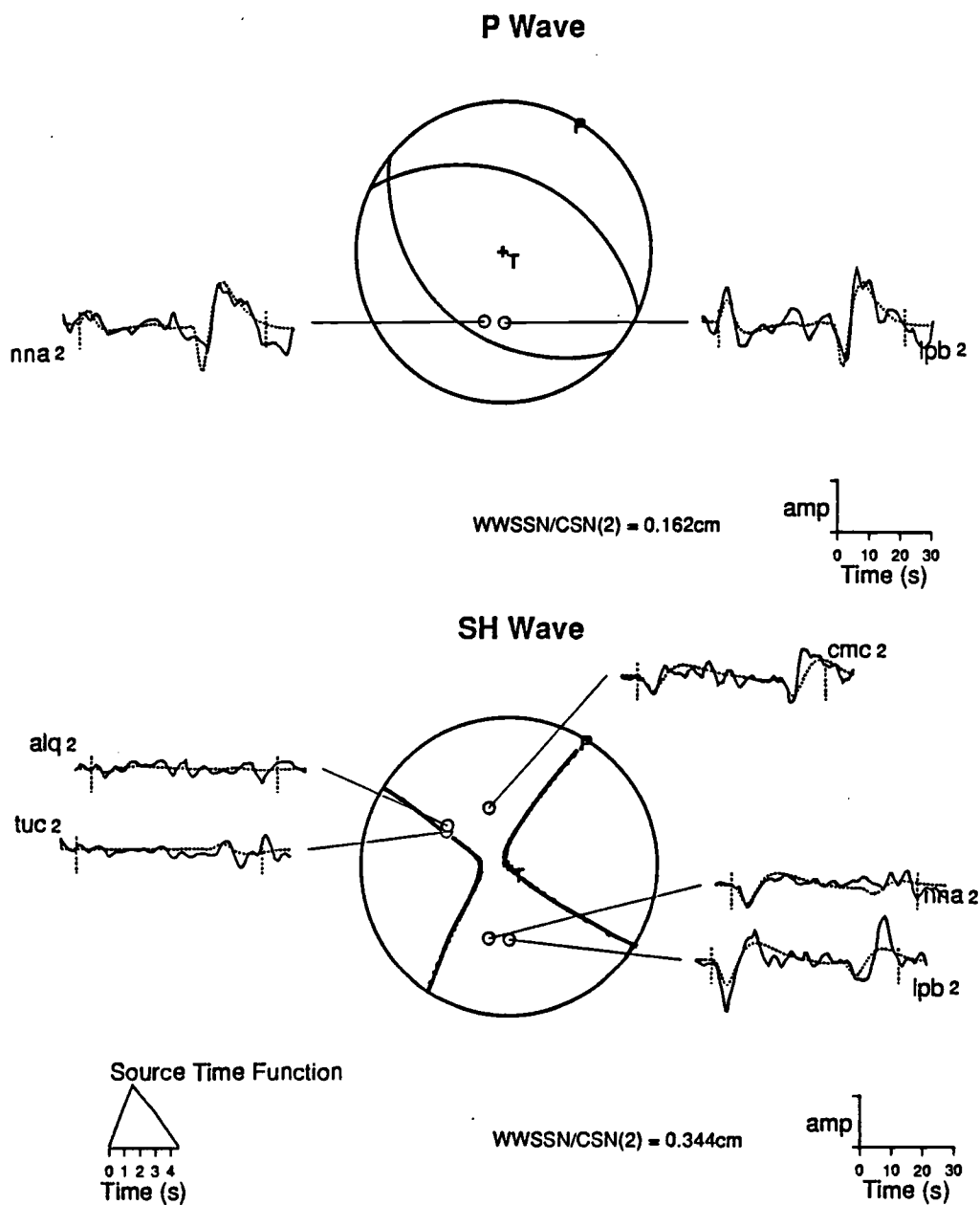
amp

0 10 20 30
Time (s)

Figure 14. Fault plane solution from inversion for Event 12/22/64

thrust event. The compressional-tensional axis pair lies in a north-northeast to south-southwest direction.

Molnar and Sykes (1969) conducted a P wave first motion analysis of this event by reading first arrival polarities from long-period seismograms of WWSSN and CSN. Their mechanism is similar to mine but shows a larger strike-slip component.

Event 09/14/81

Event 09/14/81 is the deepest (177 km) of the events that I studied, and is the strongest of the three deep events. Its total seismic moment is two and a half times larger than that of the event discussed previously. The epicenter is located just southeast of the coastline of the Dominican Republic. Minor damage was reported in western Puerto Rico, and it was felt as far away as the Virgin Islands (PDE report).

Figure 15 shows the inversion results. Azimuthal coverage for both P and SH phases was very good. However, two distinct station clusters, one to the northwest in western North America and the other to the northeast in Europe, could bias the solution. Therefore those stations with similar azimuths and takeoff angles were grouped and given smaller importance than the South American stations. Weights were assigned inversely proportional to the number of stations in each group. It has been shown (Nábělek et al., 1987) that this method provides reliable results since all sectors of the focal sphere are equally

09/14/81

P Wave

col 2

rcd 2

gol 2

alq 2

nna 2

lpb 2

kev 2

nur 2

tri 2

mal 2

aqu 2

lpa 2

P

+
T

WWSSN/CSN(2) = 0.543cm

amp

0 10 20 30
Time (s)

SH Wave

col 2

gol 2

alq 2

jct 2

nna 2

ant 2

kev 2

ume 2

val 2

nur 2

mal 2

tri 2

P

t

Source Time Function

0 1 2 3 4 5 6
Time (s)

WWSSN/CSN(2) = 0.890cm
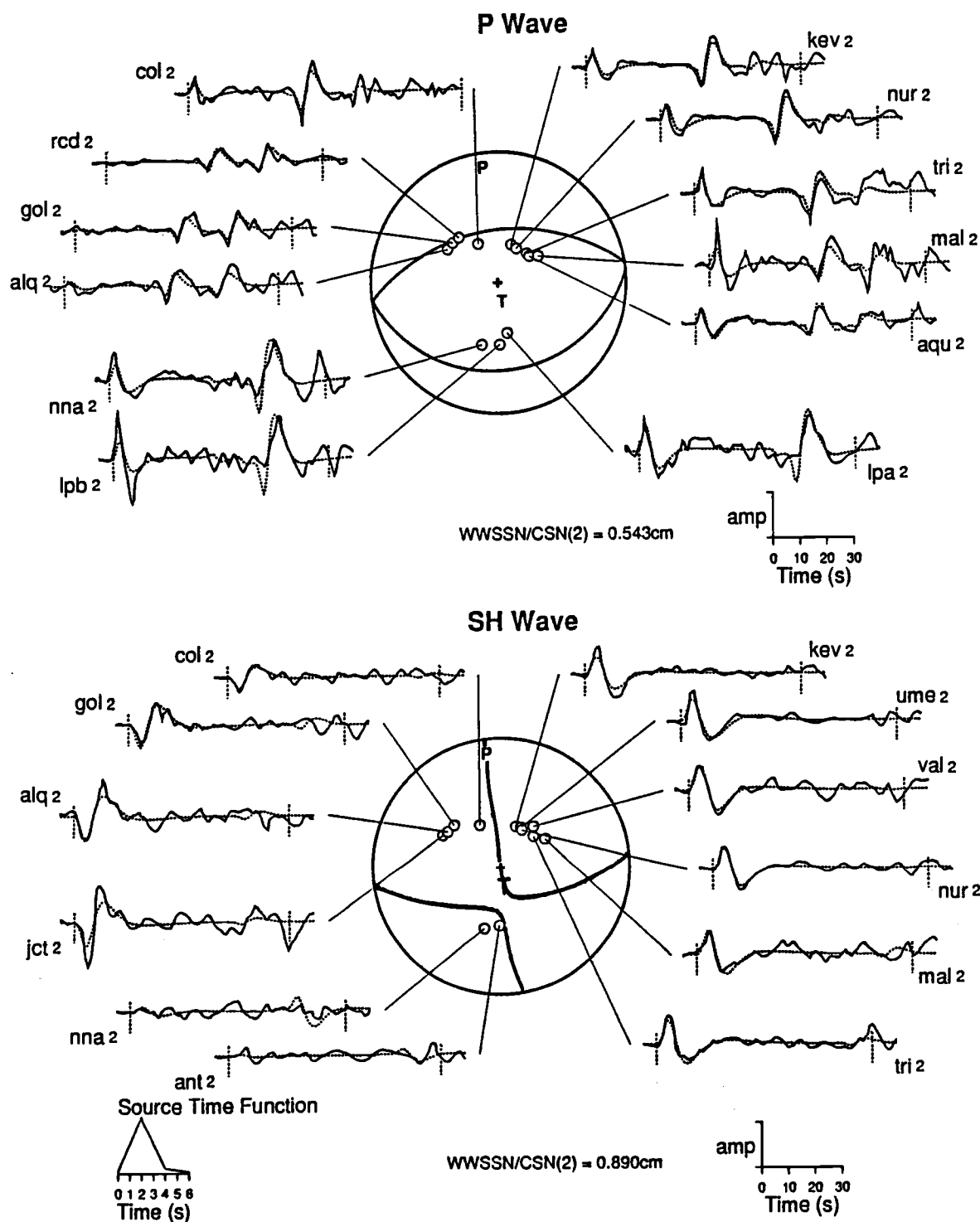
amp

0 10 20 30
Time (s)

Figure 15. Fault plane solution from inversion for Event 09/14/81

regarded. In general, the seismograms of all stations providing P waves matched very well.

The weighting scheme for SH waves was similar to that used for P waves. An excellent fit was obtained once more between the observed seismograms and the ones obtained from the inversion . Clear positive and negative S wave first arrivals can be noticed. Only the two South American stations NNA and ANT were close to a nodal plane. Having stations close to a nodal plane is not a disadvantage, since it is the variation in amplitude as well as the polarities that constrain the mechanism. A simple source time function with two 2 s time elements was found. The mechanism is a pure thrust with north-south oriented compressional and tensional axes. The obtained centroid depth is slightly greater than as was reported by PDE, 177 km versus 170 km.
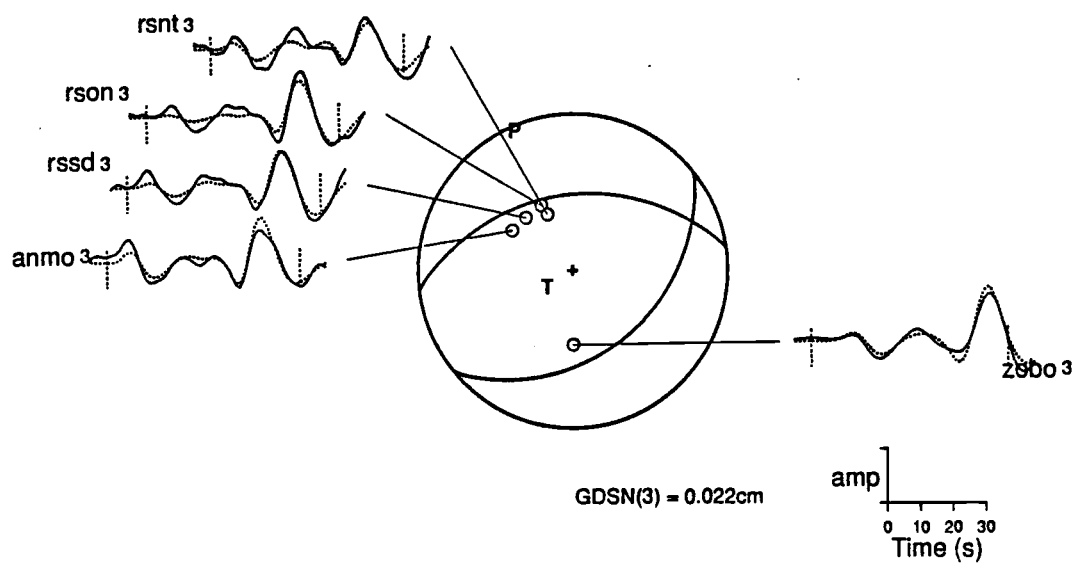
Event 09/20/83

Event 09/20/83 is the smallest and least deep of the three deep events. It provides an excellent example of the advantages of using digital GDSN data. I initially inverted using only WWSSN station data which yielded unsatisfactory results. Digital data were required to obtain constrained results for this event. Considering the uneven station distribution seen in Figure 16, I applied the same relative weights for particular seismograms as were used for Event 09/14/81.

Only digital data were used for the P waves. For the S wave data only one analog seismogram, station JCT, provided quality equal to the

09/20/83

P Wave

rsnt 3

rson 3

rssd 3

anmo 3

P

T +

zobo 3

GDSN(3) = 0.022cm

amp

0 10 20 30
Time (s)

SH Wave

rsnt 3

rson 3

rssd 3

lond 3

anmo 3

jct 2

jasd 3

kono 3

zobo 3

Source Time Function

0 1 2 3 4
Time (s)
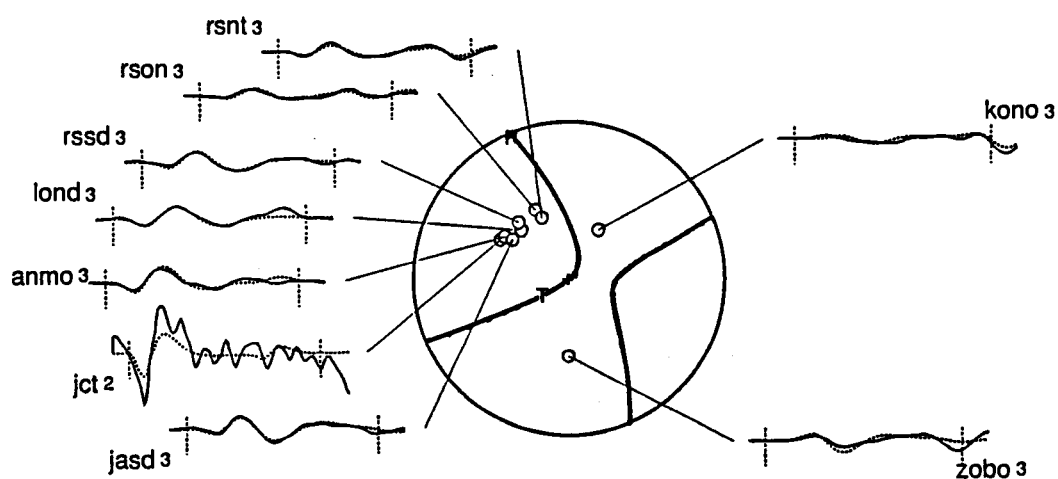
WWSSN/CSN(2) = 0.093cm
GDSN(3) = 0.108cm

amp

0 10 20 30
Time (s)
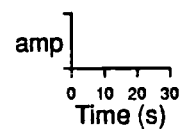
Figure 16. Fault plane solution from inversion for Event 09/20/83

digital data, and so it was included in the inversion along with a group of digital North American stations. Two important stations outside of that cluster, one in Norway (KONO) and one in Bolivia (ZOBO) provided additional constraints. The result is another thrust event with north-south compression similar to the previously discussed earthquakes, but tilted slightly more to the northwest. The source duration is 3 s.

Date	Strike [°]	Dip [°]	Slip [°]	Depth [km]	Mo [10^{17}Nm]	P-azim. [°]	P-dip [°]	T-azim. [°]	T-dip [°]
06/11/71 Event 1	282.0	73.0	97.0	59.3	8.7	6.4	27.7	202.4	61.4
	79.2	18.4	68.3						
06/11/71 Event 2	291.9±0.7	84.1±0.5	97.7±1.2	61.2±0.2	68.4±12.8	5.0	38.6	200.5	50.3
	49.3±0.7	9.7±0.5	37.7±1.2						
06/11/71 Moment Sum.	281.9±0.7	82.9±0.5	97.7±1.2	60.8±0.2	76.4±10.5	5.1	37.4	200.6	51.6
	54.7±0.7	10.5±0.5	43.3±1.2						
03/23/79 Event 1	280.0	60.0	115.0	89.2	32.9±1.1	352.2	11.6	235.7	65.3
	57.0	38.3	53.8						
03/23/79 Event 2	278.5±0.8	77.2±0.5	88.7±1.2	94.6±0.2	78.9±2.8	9.6	32.1	186.8	57.8
	104.5±0.8	12.9±0.5	95.8±1.2						
03/23/79 Moment Sum.	280.6±0.8	72.6±0.5	96.8±1.2	94.1±0.2	103.7±2.3	5.3	27.3	200.8	61.9
	79.0±0.8	18.7±0.5	69.4±1.2						
11/05/79	271.0±0.8	69.0±0.5	85.8±0.9	107.3±0.2	26.5±1.3	4.3	23.9	173.8	65.7
	102.6±0.8	21.4±0.5	100.8±0.9						

Table 5. Inversion results for intermediate events

Intermediate Events

Another group of three earthquakes (Event 06/11/71, Event 03/23/79 and Event 11/05/79) occurred at intermediate depth. Table 5 shows the final body wave inversion results for this group of events.

Event 06/11/71

For Event 06/11/71 a large number of WWSSN seismograms were available for the body wave inversion. Figure 17 shows the long-period P and SH phase seismograms that were used for the inversion.

Numerous attempts failed to provide a satisfactory fault plane solution for a single source. Nodal stations, such as TUC, ALQ and COR in North America, and ATU and TRI in southern Europe, as well as additional first motion short-period P arrivals (Figure 28), required a more southerly oriented fault plane than was obtained by inverting for one source only.

No significant directivity was observed, which would have indicated different positions for the first event and the second. However, a distinct delay in time of a second P arrival was observed at certain European and South American stations. Therefore the earthquake was inverted so that it consisted of two sub-events separated by 2 s. The first has a source time function element of 1 s and the second one has nine 1 s time elements. The results provide a fault plane solution for the first sub-event having strike and slip similar to the second subevent, but the northern fault plane is more shallow dipping at 73°. This fault plane
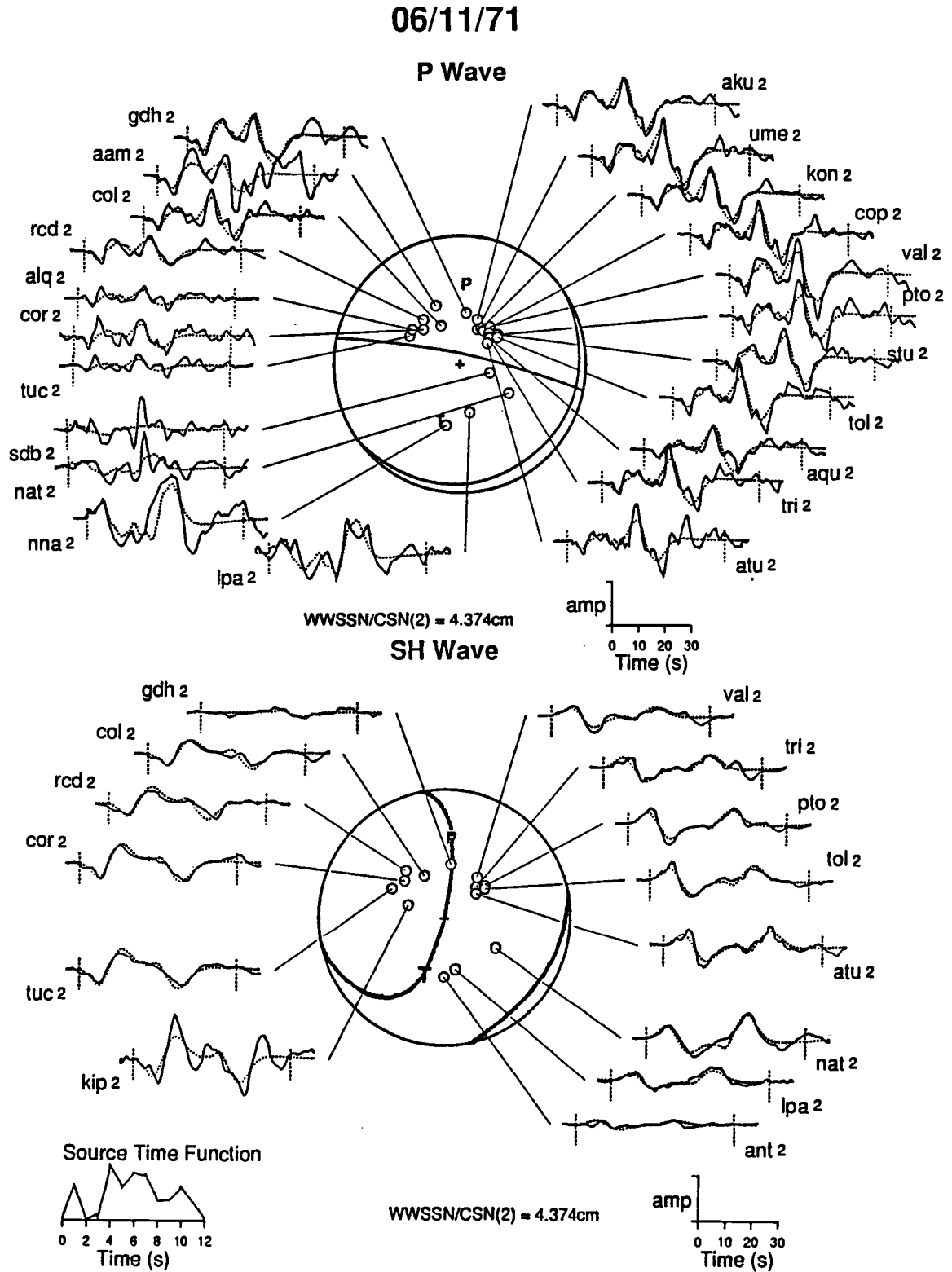
Figure 17. Fault plane solution from inversion for Event 06/11/71

solution accounts for the observed nodal character of stations in that region and is shown on Figure 28. The second fault plane solution obtained for the 2 s delayed tremor is almost identical to the one presented on Figure 17, which was obtained by moment tensor summation of the two subevents. It turned out that the energy release of the second earthquake was so much larger that it overshadowed the first one, so that the combined mechanism represents a good portrayal of the actual rupture process.

Larger weights were assigned for the P waves provided by South American stations than for stations belonging to the European or North American cluster. In general azimuthal coverage was very good, as it was for the SH waves.

The earthquake was located in the upper part of the earth's mantle, at a depth of 61 km. The mechanism is that of a steeply dipping thrust event with north-south compression only slightly inclined to the northeast.

Event 03/23/79

Event 03/23/79 is the largest magnitude earthquake to occur in the Hispaniola area in recent years. Its mechanism and the included seismograms are displayed in Figure 18. The azimuthal coverage was

03/23/79

P Wave

WWSSN/CSN(2) = 5.432cm

SH Wave

Source Time Function
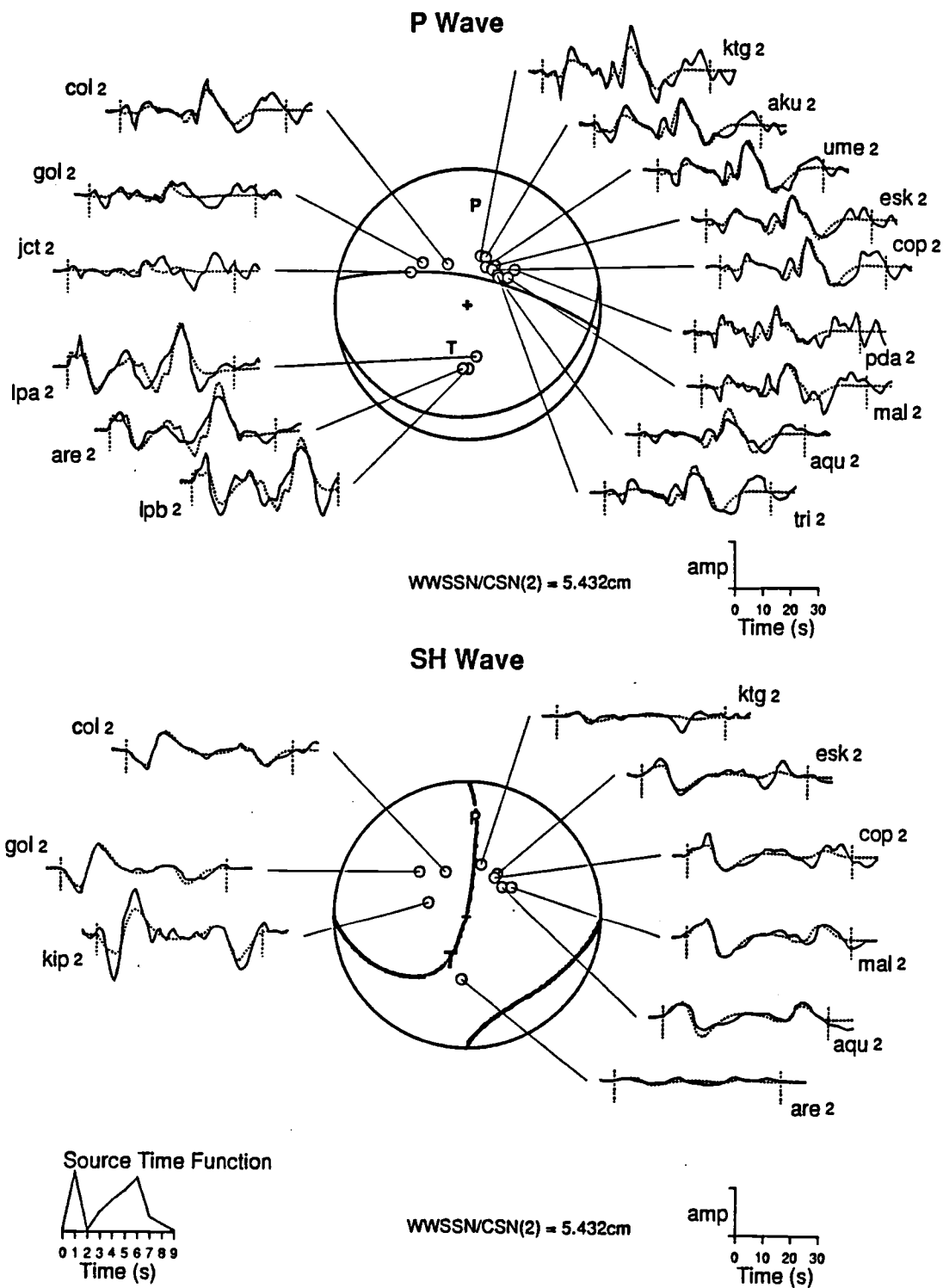
WWSSN/CSN(2) = 5.432cm

Figure 18. Fault plane solution from inversion for Event 03/23/79

good for the inversion process, with a slight bias towards the European stations, which again was accounted for by weighting.

Similar to Event 06/11/71, this event could not be successfully described using a single point source. A clear "kink" in the first P wave arrival is visible on seismograms of the South American stations LPA, LPB and ARE. This effect was not clearly observed for the North American stations, suggesting that the second rupture occurred south of the first rupture. Therefore, for the body wave inversion a second point source was assumed at 10 km south of the initial source and at a time delay of 2.5 s, which was constrained by comparison of stations LPA and LPB in particular.

In order to fit the observed first motions of long- and short-period seismograms, the first mechanism was constrained and the strike, dip and slip angles remained fixed during the inversion process for this sub-event. This fault plane solution along with the first motion polarities is shown on Figure 28. Therefore an error estimate is not given in Table 5. The second fault plane solution resulted in a greater depth and seismic moment. The northern fault plane dips more steeply but has a smaller slip angle. The solution obtained from moment tensor summation, which is shown on Figure 18 and given in Table 4, differs slightly from that of the second sub-event due to the relatively high energy release of the initial rupture. The source time function shown in Figure 18 resembles the double event. The final result for Event

03/23/79 is very similar to that of Event 06/11/71 with a steep dipping thrust mechanism.

Event 11/05/79

Event 11/05/79 is the smallest of the intermediate depth earthquakes examined. Results are presented in Figure 19 and Figure 20.

This event was suitable for an additional SV phase inversion. SV waves tend to be sensitive to crustal effects and are usable only in a limited delta range from the epicenter. Stations COL in Alaska, LOR in France and NUR in Finland provided excellent SV data.

For the P waves, the North American and European stations provided nodal or emergent first motion arrivals. However, the South American stations were evidently on the compressional plane. SH waves form groups in North and South America as well as in Europe.

The source time function consists of three elements with 1.5 s time intervals. The final solution is very consistent with that of the two previous events, indicating thrust faulting with north-south compression.
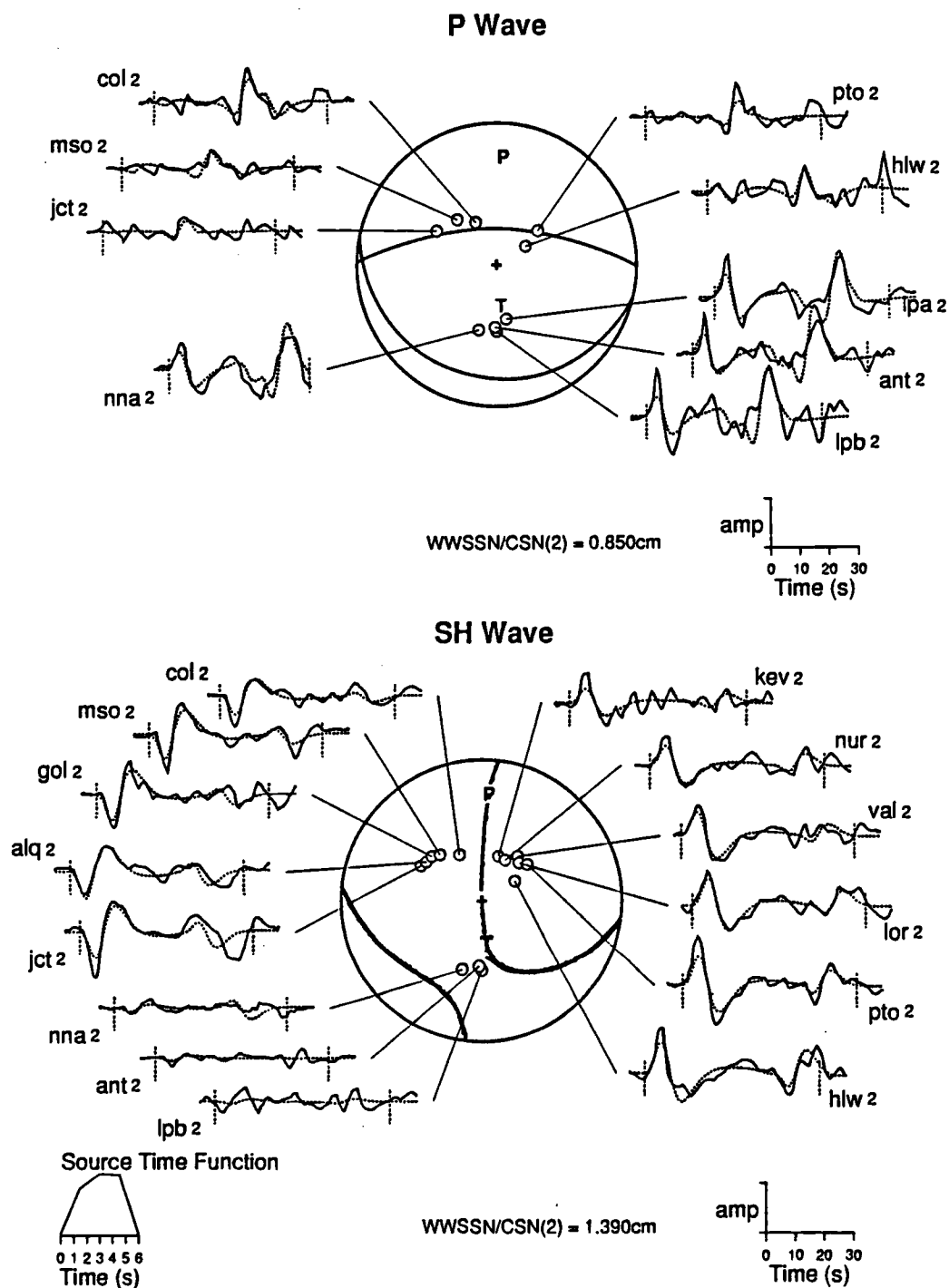
11/05/79

P Wave

WWSSN/CSN(2) = 0.850cm

SH Wave

Source Time Function

WWSSN/CSN(2) = 1.390cm

Figure 19. Fault plane solution from inversion for Event 11/05/79 (P,SH)
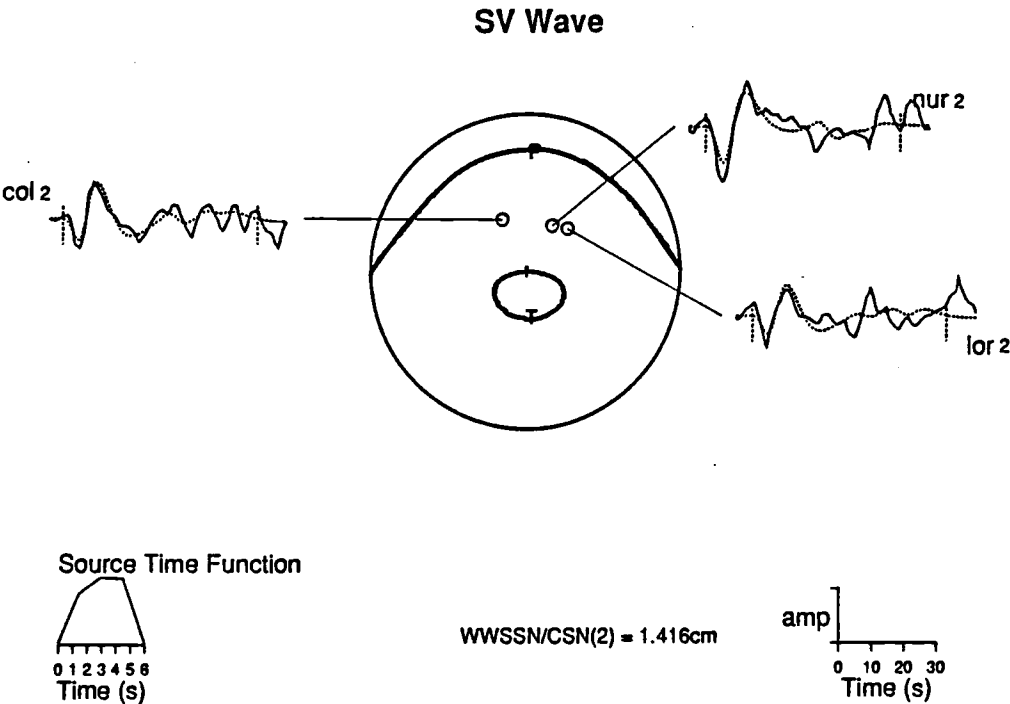
11/05/79

SV Wave

Figure 20. Fault plane solution from inversion for Event 11/05/79 (SV)

Date	Strike [°]	Dip [°]	Slip [°]	Depth [km]	Mo [10¹⁷Nm]	P-azim. [°]	P-dip [°]	T-azim. [°]	T-dip [°]
09/19/72	330.4±1.2	70.9±0.7	118.3±2.0	6.3±0.3	11.8±0.8	39.4	20.9	276.2	55.1
	91.7±1.2	33.7±0.7	36.1±2.0						
07/21/85	341.1±0.8	78.3±0.7	115.8±1.2	12.4±0.3	8.2±0.4	50.5	28.7	279.7	50.1
	93.8±0.8	28.1±0.7	25.5±1.2						
06/24/84	98.3±0.5	88.8±0.4	90.0	42.3±0.2	97.7±2.8	188.3	43.8	8.3	46.2
	278.3±0.5	1.2±0.4	90.0						
06/24/84 Halfsp.	96.8±0.5	87.8±0.4	83.5±1.7	32.7±0.2	62.7±1.9	193.0	42.5	0.0	46.8
	348.5±0.5	6.9±0.4	161.6±1.7						

Table 6. Inversion results for shallow events

Shallow Events

This group of earthquakes includes three events with depth ranging from 6 to 42 km. Their fault mechanisms are described in Table 6. Different from the two previous groups, the shallow events are located distant from one another, in different tectonic provinces.

Event 09/19/72

The epicenter of Event 09/19/72 is on land. As for Event 12/22/64, *Island Crustal Structure* was used for the body wave inversion. The epicenter is located on the Tortue-Cibao-Semana Fault Zone (Figure 2) and one would expect the event to be associated with this strike-slip feature.

Figure 21 shows the solution and data for this event. For the P phases, European stations were dilatational or emergent, while North and South American stations showed compressional first motions. Easily readable short-period P wave first arrival times provided constraint on the alignments of synthetic and observed data. The stations that provided SH waves were azimuthally well distributed and most seismograms were matched nicely. A simple three element source time function with a time element duration of 1.5 s was used.

The inversion shows that the event occurred in the upper crust. The centroid depth is 6.3 km. The mechanism shows a reverse fault with a large strike-slip component which is consistent with the epicenter location on the fault zone.
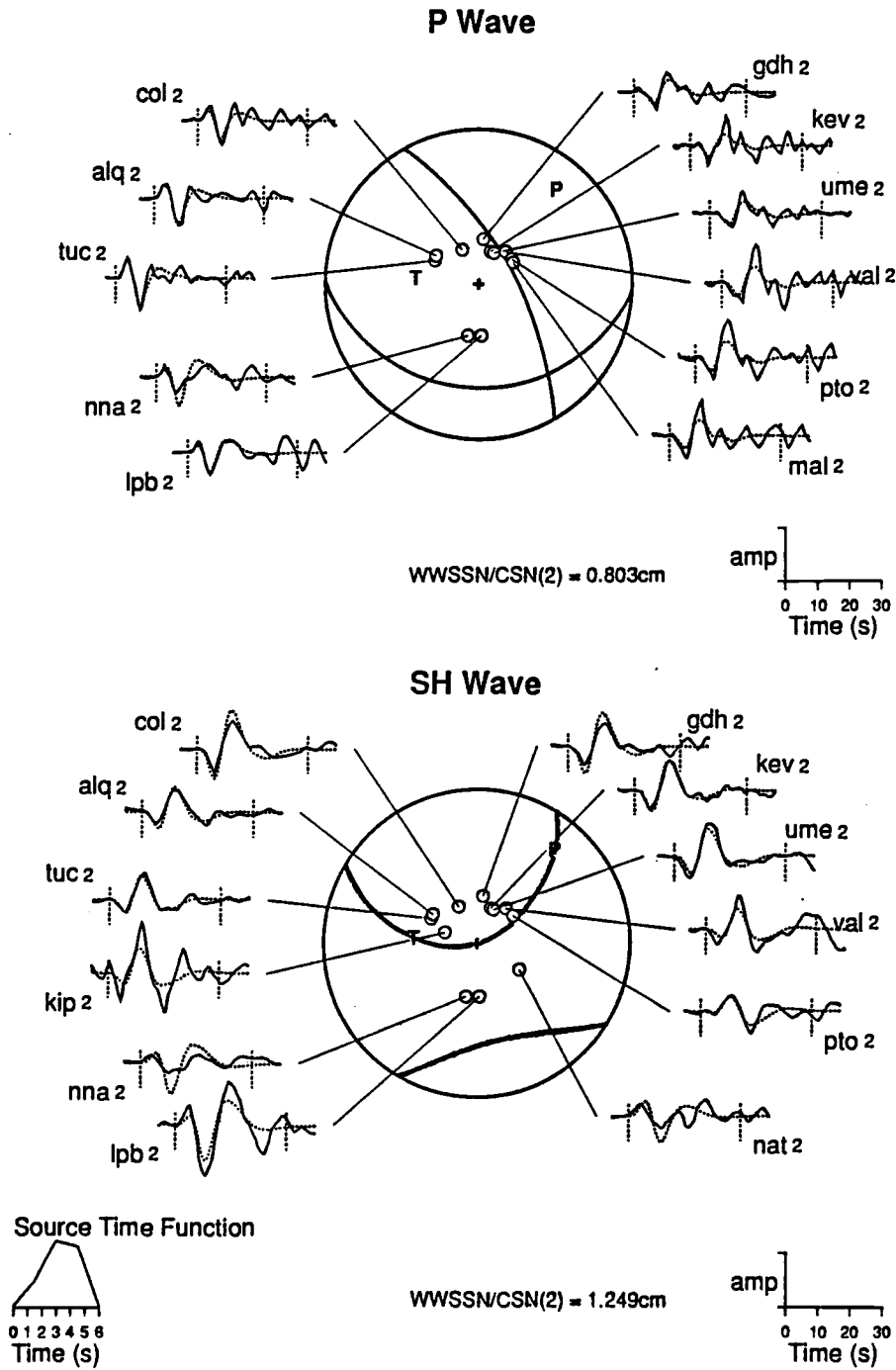
09/19/72

P Wave

col 2

alq 2

tuc 2

nna 2

lpb 2

gdh 2

kev 2

ume 2

val 2

pto 2

mal 2

P

T

+

WWSSN/CSN(2) = 0.803cm

amp

0 10 20 30
Time (s)

SH Wave

col 2

alq 2

tuc 2

kip 2

nna 2

lpb 2

gdh 2

kev 2

ume 2

val 2

pto 2

nat 2

Source Time Function

0 1 2 3 4 5 6
Time (s)

WWSSN/CSN(2) = 1.249cm

amp

0 10 20 30
Time (s)

Figure 21. Fault plane solution from inversion for Event 09/19/72
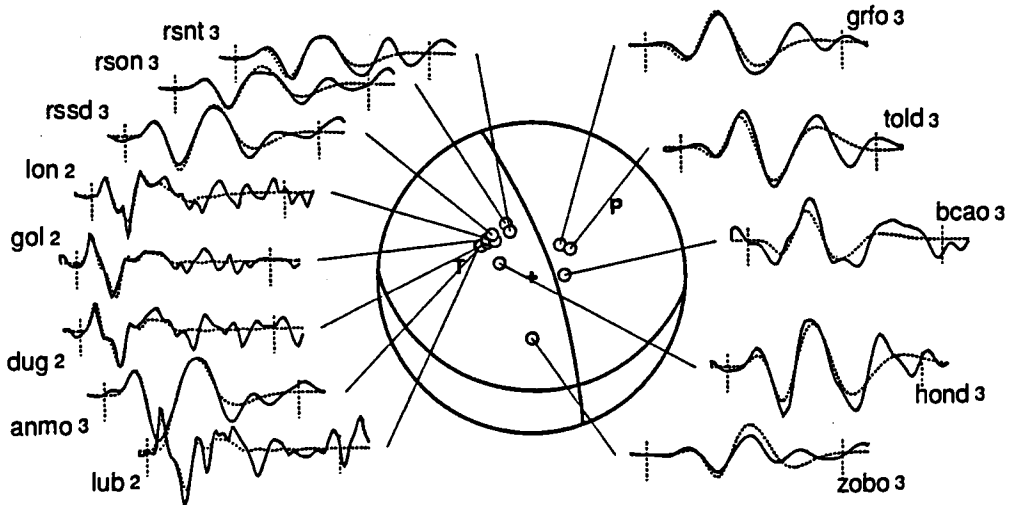
Event 07/21/85

Event 07/21/85 is another example of successful body wave inversion using combined analog and digital data. Its epicenter is located over Mona Canyon, a prominent bathymetric depression (Figure 1) between eastern Hispaniola and Puerto Rico. The fault plane solution is given in Figure 22.

Due to the small seismic moment released by this earthquake, attempts to invert this event using analog data alone were unsuccessful. Digital GDSN data helped to obtain good results. The azimuthal station coverage was sufficient, although biased by a cluster of digital stations grouped in Canada and the northern United States. To compensate, the same inverse proportional square root rule was applied. I assigned station ZOBO in Bolivia a relatively high importance appropriate to its location.
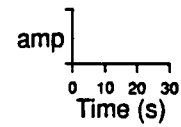
An unusually long source time function, consisting of seven 2 s time segments was needed to properly match the observed seismograms with synthetic waves. The fault plane solution is comparable to that obtained for Event 09/19/72: another reverse fault with a large strike-slip component rupturing in the crust at about 12 km depth. This is consistent with the epicenter location above an extension of the Tortue-Cibao-Semana lineament. The PDE reported depth of 35 km is clearly incorrect. The compressional-tensional axis pair lies in a northeast-southwest direction.
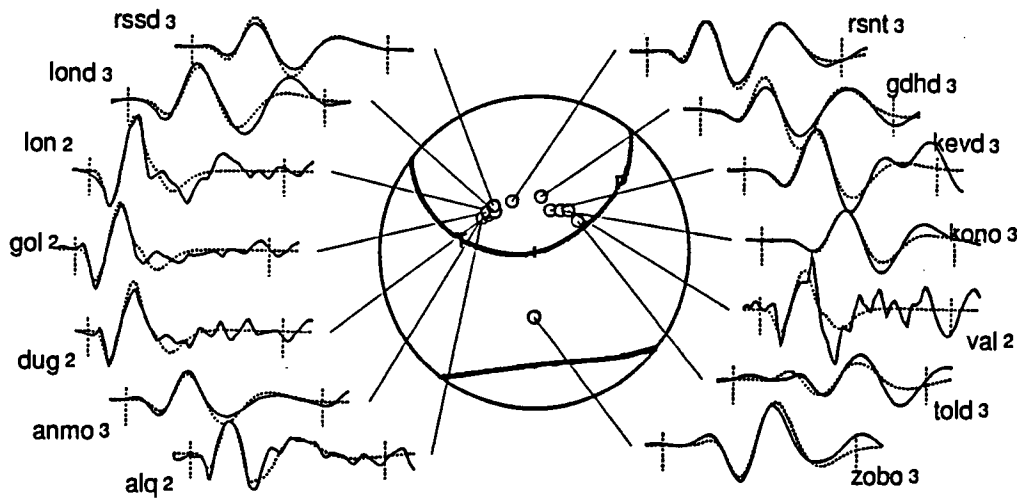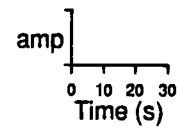
07/21/85

P Wave

rsnt 3
rson 3
rssd 3
lon 2
gol 2
dug 2
anmo 3
lub 2

grfo 3
told 3
bcao 3
hond 3
zobo 3

P

WWSSN/CSN(2) = 0.131cm
GDSN(3) = 0.057cm

amp

0 10 20 30
Time (s)

SH Wave

rssd 3
lond 3
lon 2
gol 2
dug 2
anmo 3
alq 2

rsnt 3
gdhd 3
kevd 3
kono 3
val 2
told 3
zobo 3

Source Time Function

0 2 4 6 8 10 12 14 16
Time (s)

WWSSN/CSN(2) = 0.202cm
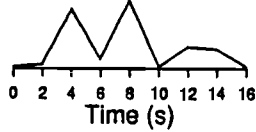GDSN(3) = 0.239cm

amp

0 10 20 30
Time (s)

Figure 22. Fault plane solution from inversion for Event 07/21/85

Event 06/24/84

In June 1984 a large earthquake occurred just southeast of Hispaniola, beneath the Muertos Trench, causing damage and casualties in the southern Dominican Republic. Event 06/24/84 was already studied by Byrne et al. (1985) using the body wave inversion technique with a limited data set. However their assumed crustal structure was a half-space, one-layer crustal model.

For comparison I inverted this event using my better constrained crustal model as well as a half space model. Figure 23 shows the data, analog and digital, that were used for the inversion and represents the solution obtained using the *Offshore Crustal Structure*. Forty seismograms (21 for P waves and 19 for SH waves) are included. The solution had to be constrained at a slip angle of 90°, since repeated inversions yielded ambiguous slip angle values in the vicinity of 90°, if it was given the same degree of freedom as the other source parameters. The compressional and dilatational planes of this event are the reverse of nearby events, such as Event 06/11/71, Event 03/23/79 and Event 09/14/81. The compressional P- and tensional T-axis pair is still north-south oriented but is also reversed.

The source time function has six elements with 2 s intervals. Most of the data, especially first P and SH motions, are matched well. Azimuthal coverage was clustered, but well distributed.
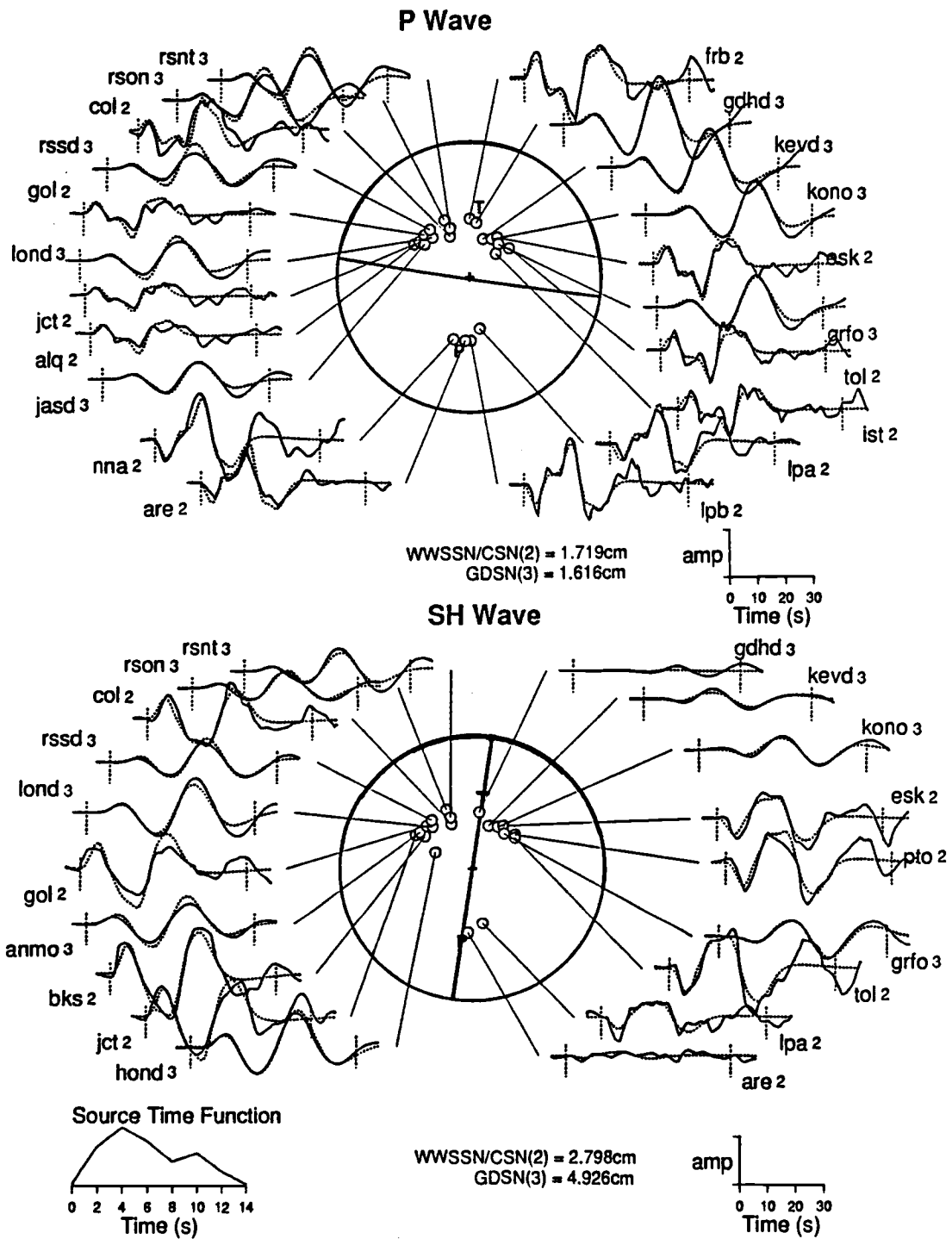
Figure 23. Fault plane solution from inversion for Event 06/24/84

The inverted centroid depth is 42.3 km, deeper than the PDE 24 km and Byrne et al.'s 32 km. To demonstrate the importance and sensitivity of a more realistic crustal structure model, I reinverted the data using a half-space, one-layer crustal model. The obtained mechanism did not change much and is given in Table 6. However, the depth was reduced from 42.3 km to 32.7 km, matching the depth by Byrne et al. Their fault plane solution showed a lower dip angle, and is probably less well constrained due to the fact that they used considerably less data for their inversion.

Summary

Figure 24 shows in map view all of the fault plane solutions obtained through body wave inversion. Two events, Event 07/21/85 and Event 06/24/84, belong to a different depth range than what was reported by PDE. Since their depth values were presented in Figure 13, the grey-shade pattern of those events changed in Figure 24. The black and white circles represent the same lower hemisphere projections as in Figures 14 to 23. Using common conventions, the compressional quadrant is black and the tensional quadrant is white. Positions of P- and T-axis are indicated.

Figure 24 also provides another look at the three different groups of events. The three deep earthquakes (Event 12/22/64, Event 09/14/81 and Event 09/20/83) show similar thrust mechanisms at the southeast tip of Hispaniola, with mostly north-south compression. They are surrounded to the south by the intermediate depth events (Event 06/11/71, Event 03/23/79 and Event 11/05/79), which also show thrust mechanisms but have a steeper dip angle. Event 06/24/84, which is among the group of intermediate events, obviously does not have a similar mechanism and is probably not related to the same tectonic feature.

To the north, two events show similar fault plane solutions representing a reverse fault with a large strike-slip component. Although they are far apart geographically, they have similar mechanisms.
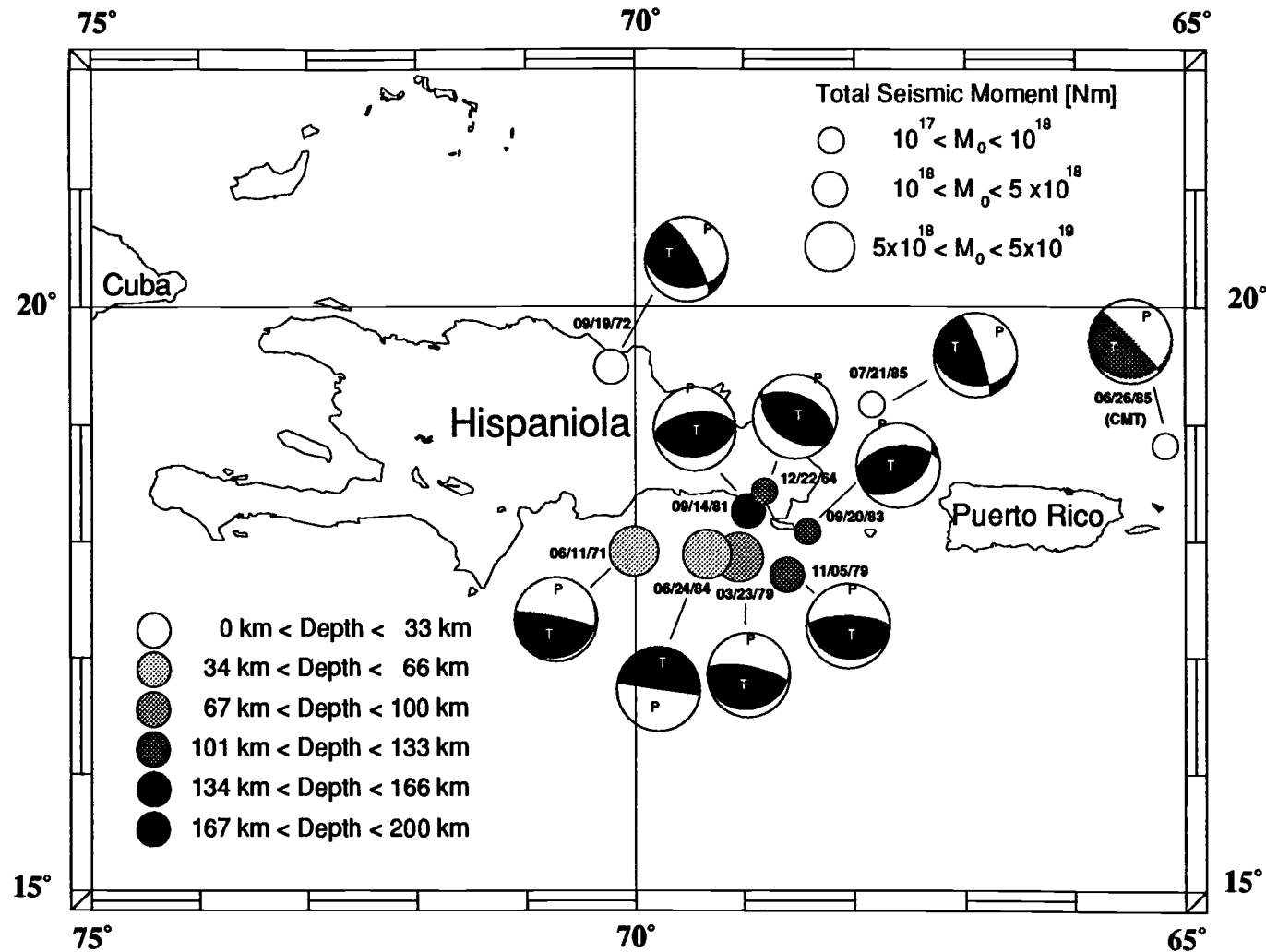
Figure 24. Fault plane solutions from body wave inversion

The grey-shaded fault plane solution shown in Figure 24 was determined by the Centroid Moment Tensor (CMT) method at Harvard. This event had a seismic moment larger than 10^{17} Nm and occurred in the Virgin Islands on 06/26/85. The centroid depth was 27 km. The mechanism is similar to my results for Event 09/19/72 and Event 07/21/85.

CONCLUSIONS

To understand the tectonic significance of the inversion results, it is first necessary to understand the meaning of the two principal stress axes, the compressional P-axis and the tensional T-axis. Isacks et al. (1968) show that for deep and intermediate earthquakes the axes of maximum compressive stress, the P-axes, are parallel to the dip of the seismic zone. The axes of least stress, the T-axes, tend to be perpendicular to the seismic zone. This means that the actual slip planes and slip directions are nonparallel to the seismic zone and therefore meaningless for the determination of slab locations and directions. Figure 25 illustrates the distribution of compressional axes (shown by a converging pair of arrows) and tensional axes (shown by a diverging pair of arrows) on a vertical profile of a subducting slab. The circles represent the sense of motion for both of the possible fault planes.

It is possible that parts of the slab might be under compression while other parts are under tension, depending upon the depth and physical or chemical changes in the subducting slab. Therefore it is necessary to examine the Hispaniola area earthquakes by projecting their P- and T- axes on a vertical profile.

Figure 26 is a vertical profile corresponding to profile 1 (Figure 4). The location of the studied events are given by shaded circles and
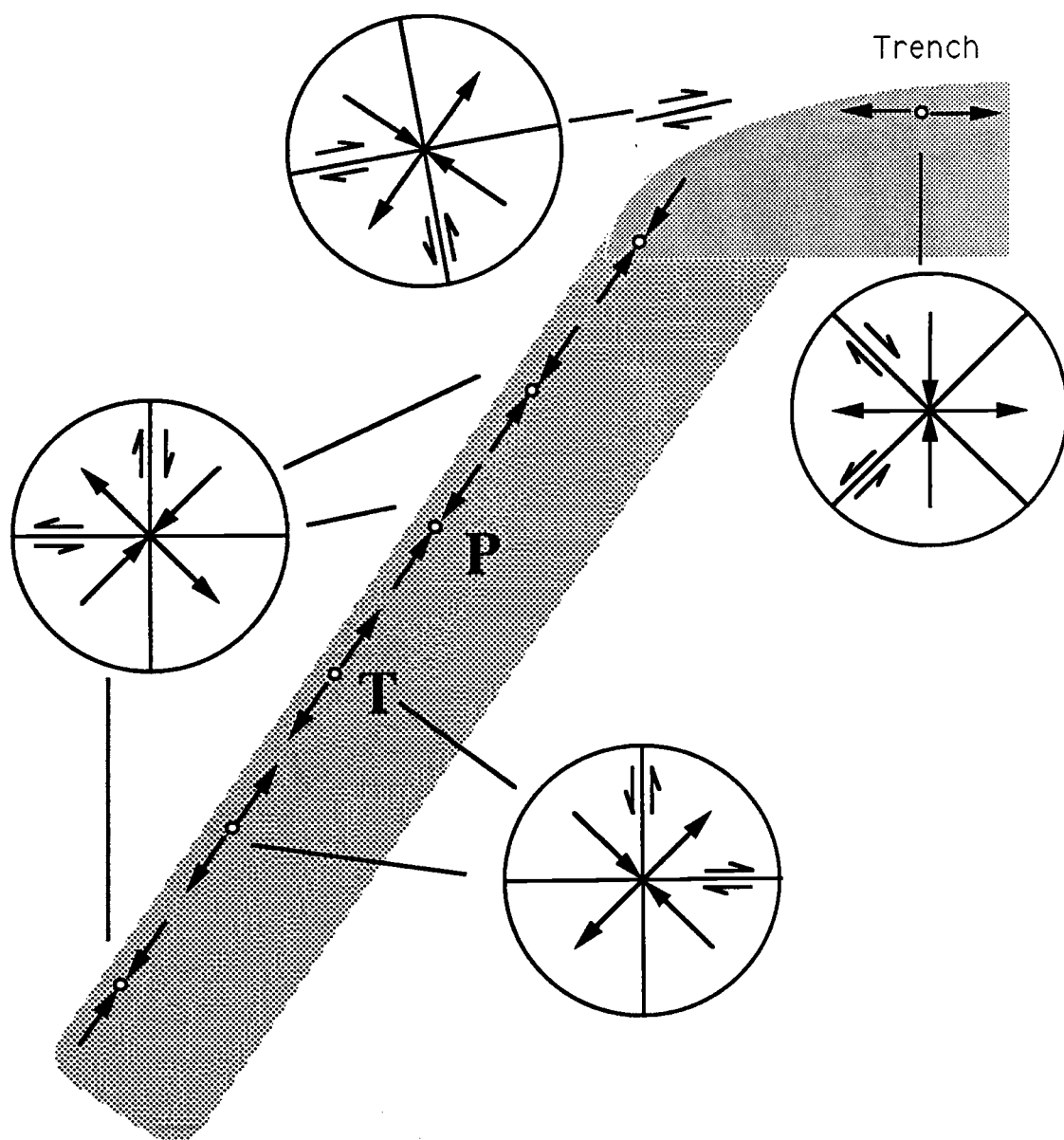
Figure 25. Vertical profile of subducting slab and the distribution of P-axes and T-axes; modified after Isacks et al. (1968)
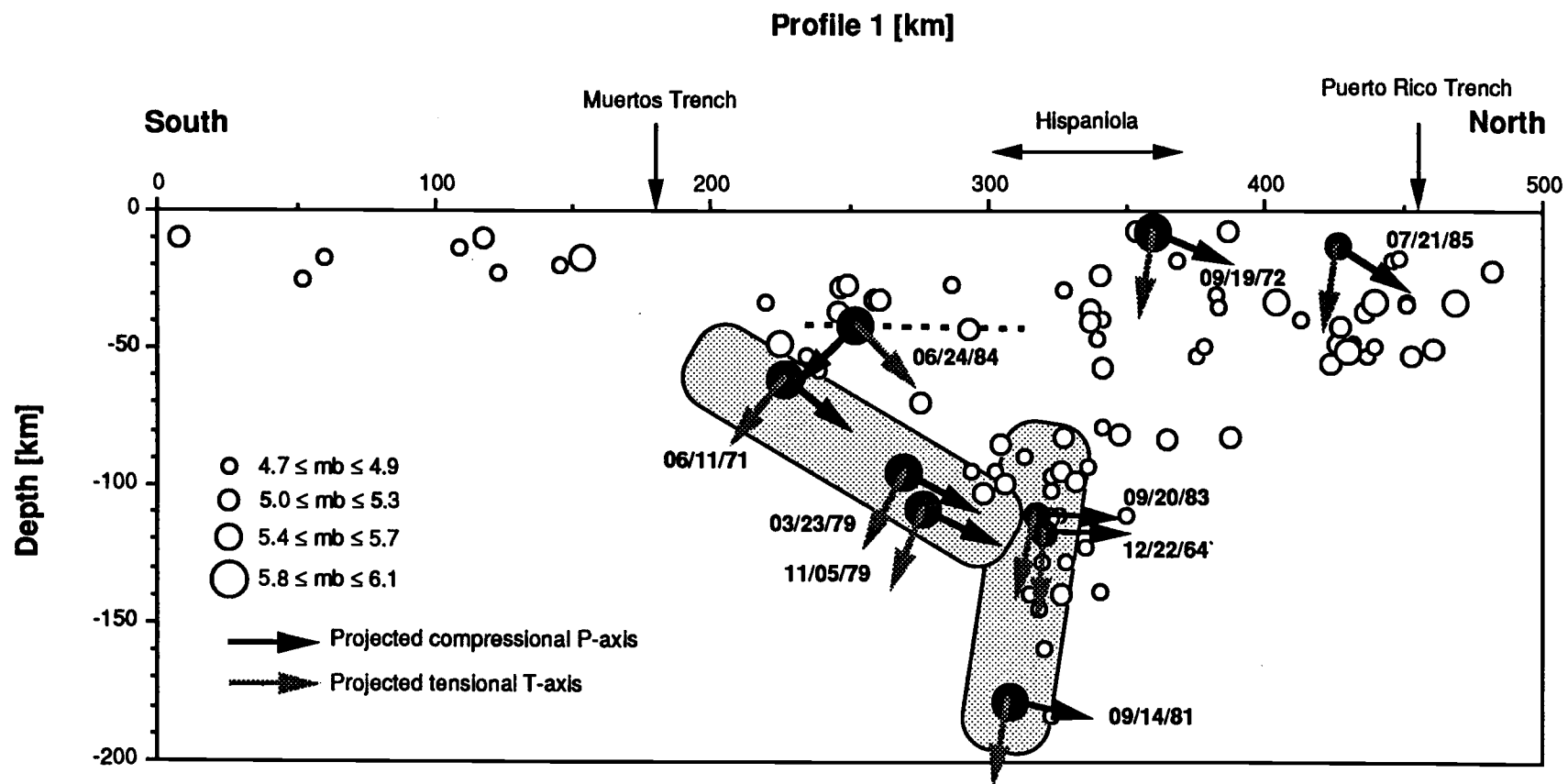
Figure 26. Vertical seismicity profile 1 (azimuth = 20°) beneath eastern Hispaniola with
P and T axes distribution of the studied events including a tectonic interpretation

can be identified by their date. The compressional P-axes and the tensional T-axes of the studied event were projected onto a vertical profile striking 20° to the northeast, perpendicular to the Puerto Rico and the Muertos trenches.

A possible tectonic interpretation is also shown in Figure 26. The three deep events show a very similar direction of their tensional axes, plunging steeply from the north. These events can be interpreted as occurring in an almost vertical slab segment, where the T-axes define the dip of the slab. At a depth of about 110 km this deep part of a slab seems to collide with another more gently dipping slab from the south, which includes the three intermediate depth earthquakes. These all have northward oriented P-axes dipping at an angle of about 30° to the north. Event 06/24/84 seems to be some kind of interface event between the overriding and the subducting plates, illustrated by a dashed line on Figure 26. The two other shallow events represent crustal deformation, probably related to strike-slip faulting at the North American-Caribbean Plate boundary. The focal mechanism of the CMT event illustrated on Figure 24 is similar to these two events.

Subduction from the south beneath eastern Hispaniola is well defined. The consistency of the compressional-tensional axes pair constrains the dip of this slab to about 30°. The occurrence of an interface event at the top of this slab segment in the upper mantle is not unusual. Similar events have been observed at other subduction zones around the world. Although there is a gap in seismic activity between

the intermediate depth earthquakes and shallow crustal events in the south, I interpret my results as an indication that the Muertos Trench is active.

An interpretation of the deep vertical slab is more difficult. One possibility is that this part of the slab represents a detached remnant of an earlier subduction that began beneath the Puerto Rico Trench. For unknown reasons, this slab segment might not be connected to the more shallow events towards the north, thus explaining the steeply inclined offset in dip angle. Another possibility is that this segment is actually connected to events occurring beneath the Puerto Rico Trench and is somehow being inflected by forces originating from the collision with the subducting slab from the south. A third interpretation is that the vertical slab is continuous with the gently dipping slab from the south. However, this would indicate that, at a depth of about 110 km, the dip of the slab would change drastically and at greater depths it would be inclined more steeply than 90° with respect to the direction of subduction. This is kinematically possible but is observed nowhere else in the world.

A more detailed analysis of earthquakes associated with the Puerto Rico Trench and investigations of future events will be necessary to confirm or rule out the possible tectonic interpretations.

BIBLIOGRAPHY

Aki, K., and P. G. Richards, *Quantitative Seismology: Theory and Methods*, vol.1, W.H. Freeman, San Francisco, Calif., 1980.

Barday, R. J., Structure of the Panama basin from marine gravity data, *M.S. Thesis*, Oregon State University, 99 pp., 1974.

Biju-Duval, B., G. Bizon, A. Mascle, and C. Muller, Active margin processes: Field observations in southern Hispaniola, *Mem. American Association of Petroleum Geologists, 34*, p. 325-344, 1982.

Bowin, C. O., The geology of Hispaniola, in *The Ocean Basins and Margins: The Gulf of Mexico and the Caribbean*, edited by A. E. M. Nairn and F. G. Stehli , p. 501-552, 1975.

Bracey, D. R., and P. R. Vogt, Plate tectonics in the Hispaniola area, *Geol. Soc. Am. Bull., 81*, p. 2855-2860, 1970.

Byrne, D. B., G. Suarez, and W. R. McCann, Muertos Trough subduction–microplate tectonics in the northern Caribbean?, *Nature, 317*, No. 6036, p. 420-421, 1985.

Case, J. E., and T. L. Holcombe, Geologic-tectonic map of the Caribbean region, *U.S. Geological Survey Miscellaneous Investigation Map 1-1100*, 1980.

DeMets, C., R. G. Gordon, D. F. Argus, and S. Stein, Current plate motions, *Geophys. Journ. Roy. Astr. Soc.*, 1989, in press.

Dillon, W. P., K. M. Scanlon, J. A. Austin Jr., N. T. Edgar, L. M. Parson, and G. E. Ness, Morphology, structure and active tectonism of the insular margin off northwestern Hispaniola, *Trans. Caribb. Geol. Conf., 12th*, 1989, in press.

Ewing, J., J. Antoine, and M. Ewing, Geophysical measurements in the western Caribbean Sea and in the Gulf of Mexico, *J. Geophys. Res., 65*, p. 4087-4126, 1960.

Holcombe, T. L., P. R. Vogt, J. E. Matthews, and R. R. Murchison, Evidence for sea-floor spreading in the Cayman Trough, *Earth Planet. Sci. Lett., 20*, p. 357-371, 1973.

Isacks, B., J. Oliver, and L. R. Sykes, Seismology and the new global tectonics, *J. Geophys. Res., 73*, p. 5855-5899, 1968.

Jordan, T. H., The present-day motions of the Caribbean plate, *J. Geophys. Res., 80*, p. 4433-4449, 1975.

Ladd, J. W., J. L. Worzel, and J. S. Watkins, Multifold seismic reflection records from the northern Venezuela Basin and the north slope of of the Muertos Trench, in *Island arcs, deep sea trenches and backarc basins, Am. Geophys. Union*, p. 41 - 56, 1977.

Ludwig, W. J., K. E. Nafe, and C. L. Drake, Seismic refraction, in: *The Sea*, v. 4, Part I, A. Maxwell (ed.), New-York, John Wiley and Sons, Inc., 53-84, 1970.

Ludwig, R., G. Ness, R. Couch, and P. Dauphin, A marine geophysical survey and modeled crustal section of Hispaniola , *EOS, 69*, No. 16, p. 462, 1988.

Mann, P., and K. Burke, Neotectonics of the Caribbean, *Rev. Geophys. and Space Phys., 22*, p. 309 - 362, 1984.

Mann, P., K. Burke, and T. Matumoto, Neotectonics of Hispaniola: Plate motion, seismicity and sedimentation at a restraining bend, *Earth Planet. Sci. Lett., 70*, p. 311-324, 1984.

McCann, W. R., and L. R. Sykes, Subduction of aseismic ridges beneath the Caribbean plate: Implications for the tectonics and seismic potential of the northeastern Caribbean, *J. Geophys. Res., 89*, p. 4493-4519, 1984.

Minster, J. B., and T. H. Jordan, Present-day plate motions, *J. Geophys. Res., 83*, p. 5331-5354, 1978.

Molnar, P., and L. Sykes, Tectonics of the Caribbean and Middle America regions from focal mechanisms and seismicity, *Geol. Soc. Am. Bull.*, v. 80, p. 1639 -1684, 1969.

Nábělek, J. L., Determination of earthquake source parameters from inversion of body waves, *Ph. D. Thesis*, Mass. Inst. of Tech., Cambridge, Mass., 361 pp., 1984.

Nábělek, J., The Tangshan earthquake sequence and its implications for the evolution of the North China Basin, *J. Geophys. Res., 92*, p. 12615-12628, 1987.

Perfit, M. R., B. C. Heezen, M. R. Rawson, and T. W. Donnelly, Chemistry, origin and significance of metamorphic rocks from the Puerto Rico Trench, *Mar. Geol., 34*, p. 125-156, 1980.

Perry, R. K., Bathymetry of the Gulf of Mexico and the Caribbean Sea, *The American Association of Petroleum Geologists*, 1984.

Saunders, J. G., P. Jung, J. Geister, and B. Biju-Duval, The Neogene of the South Flank of the Cibao Valley, Dominican Republic: A stratigraphic study, *Trans. Caribb. Geol. Conf., 9th*, p. 151-160, 1980.

Shepherd, J. B. and W. P. Aspinall, Seismicity and seismic intensities in Jamaica, West Indies: A problem in risk assessment, *Earthquake Eng. Struct. Dyn., 8*, p. 315-335, 1980.

Stein, S., C. DeMets, R. G. Gordon, J. Brodholt, J. F. Engeln, D. A. Wiens, D. Argus, P. Lundgren, C. Stein, and D. Woods, A test of alternative Caribbean plate relative motion models, *J. Geophys. Res., 93*, p. 3041-3050, 1988.

Stephan, J. F., R. Blanchet, and B. Mercier de Lepinay, Northern and southern Caribbean festoons (Panama, Colombia–Venezuela and Hispaniola–Puerto Rico), interpreted as pseudosubductions induced by the east-west shortening of the peri-Caribbean continental frame in *The Origin of Arcs*, edited by F.-C. Wezel, p. 401-422, 1986.

Sykes, L. R., W. R. McCann, and A. L. Kafka, Motion of Caribbean plate during last 7 million years and implications for earlier Cenozoic movements, *J. Geophys. Res., 87*, p. 10656-10676, 1982.

Talwani, M., and J. R. Heirtzler, Computation of magnetic anomalies caused by two-dimensional structures of arbitrary shape, in *Computers in the mineral industries*, G. A. Parks, Ed., Stanford University, p. 464-480, 1964.

Talwani, M., J. L. Worzel, and M. Landisman, Rapid gravity computations for two-dimensional bodies with application to the Mendocino submarine fracture zone, *Journal of Geophysical Research, 64*, p. 49-59, 1959.

Tomblin, J. F., The Lesser Antilles and the Aves Ridge, in *The Ocean Basins and Margins: The Gulf of Mexico and the Caribbean*, edited by A. E. M. Nairn and F. G. Stehli , p. 467-500, 1975.

Wadge, G., and K. Burke, Neogene Caribbean plate rotation and associated Central American tectonic evolution, *Tectonics, 2*, p. 633-643, 1983.
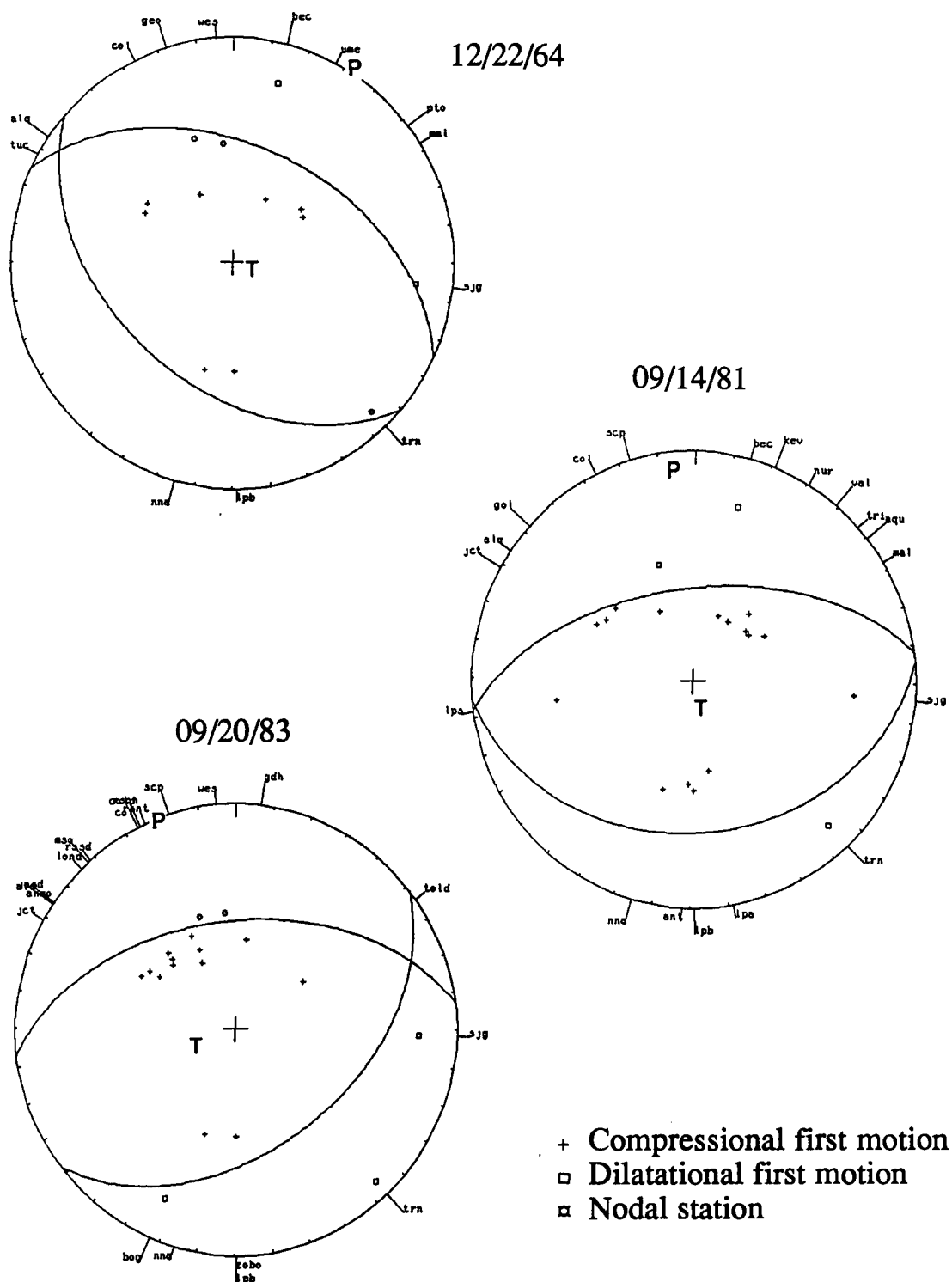
APPENDIX
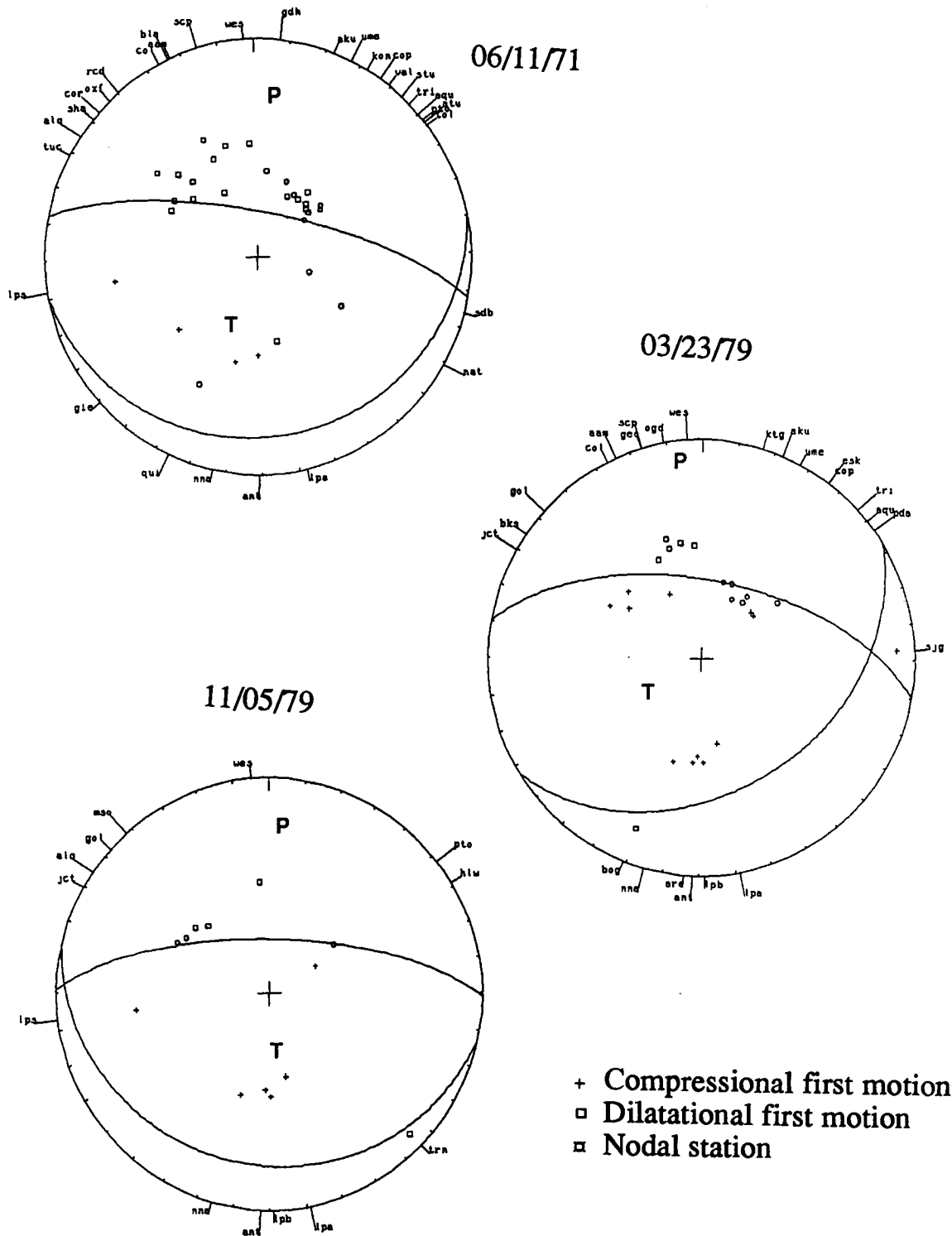
Figure 27. First motion polarities for deep events
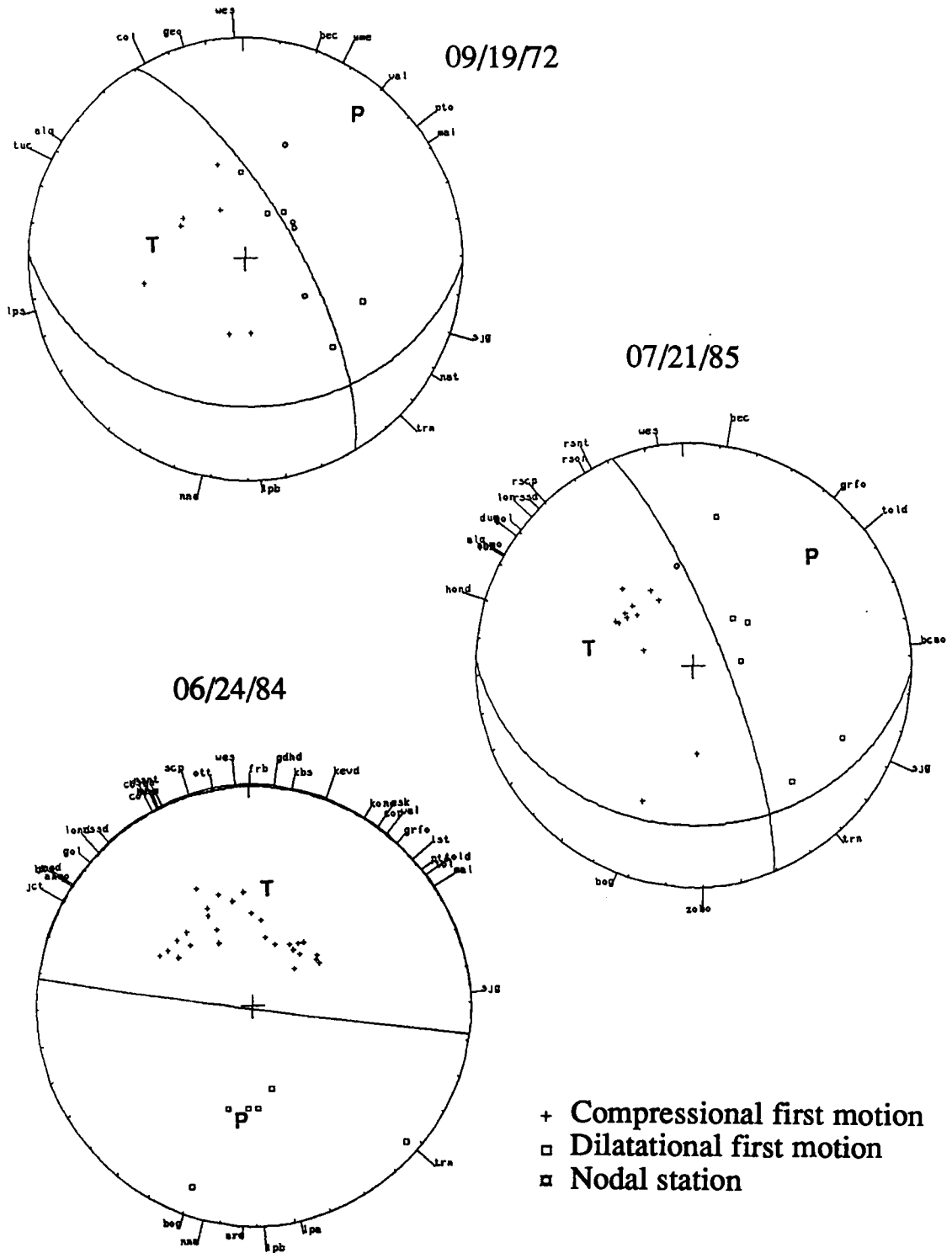
Figure 28. First motion polarities for intermediate events

Figure 29. First motion polarities for shallow events